

Accepted Article

Is Turning Down the Sun a Good Proxy for Stratospheric Sulfate Geoengineering?

Daniele Visioni¹, Douglas G. MacMartin¹, Ben Kravitz^{2,3},

¹Sibley School for Mechanical and Aerospace Engineering, Cornell University, Ithaca, NY

²Department of Earth and Atmospheric Sciences, Indiana University, Bloomington, IN

³Atmospheric Sciences and Global Change Division, Pacific Northwest National Laboratory, Richland, WA, USA

Key Points:

- Reducing the incoming solar radiation is often used to emulate injecting SO₂ in the stratosphere, but produces different surface outcomes
- Solar reduction matched to the pattern produced by the aerosol optical depth results in better surface climate matching between the methods
- Including the stratospheric heating produced by the aerosols produces further improvements and highlights key physical mechanisms at play

Corresponding author: Daniele Visioni, daniele.visioni@cornell.edu

This article has been accepted for publication and undergone full peer review but has not been through the copyediting, typesetting, pagination and proofreading process, which may lead to differences between this version and the [Version of Record](#). Please cite this article as [doi: 10.1029/2020JD033952](https://doi.org/10.1029/2020JD033952).

This article is protected by copyright. All rights reserved.

Abstract

Deliberately blocking out a small portion of the incoming solar radiation would cool the climate. One such approach would be injecting SO₂ into the stratosphere, which would produce sulfate aerosols that would remain in the atmosphere for 1–3 years, reflecting part of the incoming shortwave radiation. The cooling produced by the aerosols can offset the warming produced by increased greenhouse gas (GHG) concentrations, but it would also affect the climate differently, leading to residual differences compared to a climate not affected by either. Many climate model simulations of geoengineering have used a uniform reduction of the incoming solar radiation as a proxy for stratospheric aerosols, both because many models are not designed to adequately capture relevant stratospheric aerosol processes, and because a solar reduction has often been assumed to capture the most important differences between how stratospheric aerosols and GHG would affect the climate. Here we show that dimming the sun does not produce the same surface climate effects as simulating aerosols in the stratosphere. By more closely matching the spatial pattern of solar reduction to that of the aerosols, some improvements in this idealized representation are possible, with further improvements if the stratospheric heating produced by the aerosols is included. This is relevant both for our understanding of the physical mechanisms driving the changes observed in stratospheric-sulfate geoengineering simulations, and in terms of the relevance of impact assessments that use a uniform solar dimming.

Plain Language Summary

Injecting SO₂ in the stratosphere has been proposed as a method to temporarily cool the planet by partially reflecting the incoming solar radiation. To assess the eventual side-effects of this method, some climate model simulations have simply reduced the solar constant in the model rather than simulating the actual aerosols that would be produced. We show here what the limits of emulating stratospheric sulfate injection this way are, and what are the physical causes behind the differences from simulations where stratospheric aerosols are simulated.

1 Introduction

The possibility of injecting SO₂ in the stratosphere to mitigate some of the negative effects of anthropogenic global warming has been discussed for decades, starting with Budyko (1978) and notably by Crutzen (2006). Despite model simulations showing that it would be effective at offsetting many aspects of climate change (e.g. Kravitz et al., 2017; P. J. Irvine & Keith, 2020), deploying stratospheric sulfate (SS) injections would come with drawbacks of its own, and many studies have explored the possible side effects of this method, both in the stratosphere (Tilmes et al., 2008; Pitari et al., 2014) and at the surface (Jones et al., 2018; Jiang et al., 2019). When comparing two climates with similar global surface temperatures (or other globally-defined metrics, Lee et al. (2020)), where one is engineered with stratospheric aerosols and the other has lower CO₂, they would differ because aerosols and GHG do not affect the climate system via the same pathways: while the aerosols reduce solar radiation (shortwave; SW) at the surface, the increasing CO₂ concentrations trap more outgoing longwave radiation (LW) emitted by the planet. Moreover, the spatial and seasonal dependence of the two forcings are also different (Govindasamy et al., 2003; Ban-Weiss & Caldeira, 2010; Jiang et al., 2019), since CO₂ is a well mixed gas with relatively uniform radiative effect in both space and season, while the insolation varies strongly with latitude and season, and the spatial distribution of stratospheric aerosols also varies due to the stratospheric circulation and injection location (Tilmes et al., 2017). The net results of these effects on the surface are that while the global mean temperature could be successfully reduced through stratospheric sulfate injections, the combination of stratospheric aerosol and increased CO₂

forcing would lead to residual differences such as regional changes to the hydrological cycle (Jones et al., 2018; Simpson et al., 2019; Cheng et al., 2019). These changes, however, would very likely be smaller in magnitude than those produced by climate change itself (MacMartin et al., 2019; P. J. Irvine & Keith, 2020). Another important difference is to be found in the stratosphere, where the sulfate aerosols would absorb some near-infrared radiation and heat the air locally, resulting in changes to stratospheric dynamics (Aquila et al., 2014; Niemeier & Schmidt, 2017; Richter et al., 2017; Niemeier et al., 2020; Visioni, MacMartin, Kravitz, Lee, et al., 2020), chemistry (Visioni, Pitari, Aquila, Tilmes, et al., 2017; Tilmes, Richter, Mills, et al., 2018), and upper tropospheric clouds (Kuebbeler et al., 2012; Visioni, Pitari, Di Genova, et al., 2018). Furthermore, the stratospheric heating may also affect the surface climate due, for instance, to shifts in the atmospheric circulation (Simpson et al., 2019).

Globally, the differential impact of longwave and shortwave radiative effects has been considered to be the main reason for the surface climate differences, and so reducing the solar constant rather than actually simulating the aerosols has been a widely used simulation technique (Kravitz, Caldeira, et al., 2013). While this simplification clearly would not capture impacts such as changes in ozone (Tilmes et al., 2008) or different ratio of direct/diffuse light (Kravitz et al., 2012), it does capture the simultaneous reduction of SW radiation and increase in LW radiation. Due to the uncertainties in our understanding of stratospheric sulfate microphysics and interaction with radiation, and to the lack, in some models, of a proper representation of stratospheric circulation, this simplification has also allowed more climate models to perform similar simulations (Kravitz, Caldeira, et al., 2013). Many studies have thus used a uniform reduction of the solar constant (solar dimming, SD) as a proxy to simulate the effects of stratospheric sulfate geoengineering, looking at its consequences on surface processes, for instance on the hydrological cycle (Smyth et al., 2017; Russotto & Ackerman, 2018a, 2018b; Guo et al., 2018; Ji et al., 2018; P. Irvine et al., 2019) and vegetation (Glienke et al., 2015; Dagon & Schrag, 2019). Some recent studies aiming to generally evaluate Solar Radiation Management (SRM) techniques in the framework of Integrated Assessment Modeling have also used SD climate simulations as a proxy for any SRM method (Tavoni et al., 2017; Oschlies et al., 2017; Low & Schfer, 2019; Harding et al., 2020).

However, reducing solar irradiance instead of simulating the stratospheric aerosols would only be a good proxy if the differential SW and LW effects dominate the surface climate impacts, as this approximation does not include stratospheric warming caused by the absorption of LW radiation by the sulfate aerosols (Richter et al., 2017; Niemeier & Schmidt, 2017; Kleinschmitt et al., 2018), nor does it capture differences in the spatio-temporal distribution of the aerosols (Dai et al., 2018; Visioni et al., 2019). Furthermore, the impact of aerosols on the ratio of direct to scattered incident light would lead to changes in downwelling radiation at the surface, in turn affecting ecosystems. Previous studies have already compared the two methods and highlighted some of the differences in the surface response (Niemeier et al., 2013; Ferraro et al., 2015; Kalidindi et al., 2015; Xia et al., 2017), finding generally lower changes in the hydrological cycle when performing SD simulations compared to SS ones. However, these previous comparisons have always equated SD with a global decrease in the solar constant and SS with equatorial injections aimed at managing globally averaged quantities, either temperature or radiative forcing. Furthermore, earlier models oftentimes used either non-fully interactive or prescribed aerosols (Kalidindi et al., 2015; Xia et al., 2017) to simulate SS.

In recent years it has been shown that by combining injections at different latitudes it is possible to devise SS strategies capable of managing more than just global surface temperature (Kravitz et al., 2017). The ability of SS to be tailored to more precisely modify the distribution of the radiative forcing in order to minimize projected side effects (MacMartin et al., 2017; Dai et al., 2018; Lee et al., 2020) is therefore another important difference compared to SD.

Table 1. Summary of the simulations analyzed in this paper, with a general description of the method used to maintain surface temperatures at 2010-2030 levels. 1×1 and 3×3 indicate the climate objectives (first number) and the degrees of freedom that need to be modified in order to achieve those goals (second number) (see for further explanation Kravitz et al., 2016).

Sim. name	Description
1×1 SD	Uniform solar dimming to maintain global mean temperature
1×1 SS	Stratospheric sulfate aerosols injected at the equator to maintain global mean temperature
3×3 SD	Solar dimming in three independently adjusted patterns (globally uniform, linear with sine of latitude, and quadratic with sine of latitude) to maintain global mean temperature, the interhemispheric temperature gradient, and the equator-to-pole temperature gradient
3×3 SS	Stratospheric sulfate aerosol injection at four independent locations (30°S , 15°S , 15°N , and 30°N) to maintain global mean temperature, the interhemispheric temperature gradient, and the equator-to-pole temperature gradient
3×3 SDH	As in 3×3 SD but with the stratospheric heating patterns from 3×3 SS superimposed

In light of this, we reconsider in this work the simulated physical differences between SS and SD simulations. Together with simulations more similar to those analyzed in the past (equatorial injections and spatially uniform reduction in the solar constant) we consider here also a set of SS simulations designed to maintain, through multiple injection locations, the global surface temperature together with the inter-hemispheric and equator-to-pole gradients of temperature (Tilmes, Richter, Kravitz, et al., 2018). We also consider a new set of SD simulations designed to achieve similar objectives through a non-spatially-uniform reduction in the solar constant (similar to Kravitz et al., 2016). Finally, we also include one more set including a 3×3 SD reduction while superimposing the stratospheric heating that would be produced by the aerosols in the analogous SS simulations. A similar experiment has been performed in Simpson et al. (2019), with heating rates from stratospheric aerosols imposed for 20 years in the period 2010-2030. In our case, the simultaneous presence of the stratospheric heating and of the non-uniform solar dimming allows for a more direct comparison between the sets of experiments, given the ability to maintain similar temperature gradients compared to the SS simulations. By cross-comparing these five sets (Table 1), we aim to better separate the differences produced by the various factors mentioned above, in particular those driven by differences in the obtained temperature gradients (caused by latitudinal differences in the amount of solar radiation reflected or attenuated) and those driven by the presence of the aerosols themselves, for instance by further isolating the role of the stratospheric heating in the changes observed in the SS simulations.

This paper is structured as follows: in Section 2 we explain how the 5 sets of simulations were built, and we expand on how the cross-comparisons can clarify single aspects of the climatic response. In Section 3.1 we compare the simulated results in terms of surface temperature and precipitation and try to understand the physical mechanisms behind them, then try to quantify how well the SD simulations represent the SS ones for some of those quantities in section 3.2. We then discuss other quantities for which the response is highly different in Section 3.3 for the surface and in Section 3.4 for stratospheric quantities. Finally, we discuss our results in Section 4.

147 2 Methods

148 We analyze here 5 sets of simulations performed with the Community Earth Sys-
 149 tem Model (CESM), with the Whole Atmosphere Community Climate Model (WACCM)
 150 as its atmospheric component (Mills et al., 2017), with 70 vertical layers reaching up to
 151 140 km and comprehensive, fully-interactive stratospheric chemistry. The model also has
 152 a land component (Community Land Model, version 4.5) and coupled ocean (Parallel
 153 Ocean Program, version 2, Danabasoglu et al. (2012)) and sea ice (Los Alamos Sea Ice
 154 Model, CICE4). This configuration of the model has been thoroughly evaluated in Mills
 155 et al. (2016, 2017), and compares well with present-day and past observations, both in
 156 quiescent conditions and in the period following the 1991 Mt.Pinatubo eruption.

157 All simulations follow greenhouse gas emissions prescribed under the RCP8.5 sce-
 158 nario, and with either solar dimming or stratospheric SO₂ injections to offset the warm-
 159 ing relative to 2020 (calculated as the average over 2010–2030 from a 20-member ensem-
 160 ble of RCP8.5 simulations). The sets termed 1 × 1 aim to keep the global yearly sur-
 161 face temperature (T0) at the 2010–2030 average, either by means of a uniform reduc-
 162 tion of the solar constant (1 × 1 SD) or by SO₂ injections at the equator 5 km above
 163 the tropopause (1 × 1 SS) (Kravitz et al., 2019). The other sets, termed 3 × 3, aim to
 164 keep three surface temperature targets: keeping global yearly surface temperatures and
 165 inter-hemispheric (T1) and equator-to-pole temperature gradients at the 2010–2030 av-
 166 erage (T2), either by modifying the solar constant proportionally to constant, linear, and
 167 quadratic functions of the sine of latitude (projections of the first three Legendre poly-
 168 nomials onto area-weighted solar reduction) (3×3 SD) (see MacMartin et al., 2013; Kravitz
 169 et al., 2016) or by injecting SO₂ at 4 latitudes (30°S, 15°S, 15°N, and 30°N), 5 km above
 170 the tropopause and at the international date line, to achieve an aerosol optical depth (AOD)
 171 similar to the desired 3×3 solar reductions needed (3×3 SS) (Tilmes, Richter, Kravitz,
 172 et al., 2018). Decisions on the amount of solar reduction or on the amount of SO₂ to in-
 173 ject at each location are taken at the end of each year of simulation by a feedback loop
 174 (Kravitz et al., 2017) to ensure that the desired goals are met. Both SS sets have already
 175 been described and analyzed in Tilmes, Richter, Kravitz, et al. (2018) and Kravitz et al.
 176 (2019).

177 A final ensemble of simulations tries to maintain the three surface temperature goals
 178 with the same method as the 3 × 3 SD one, but imposes in the stratosphere the same
 179 stratospheric heating rates that would result from the stratospheric aerosols in the 3 ×
 180 3 SS simulation in the same period, with a method similar to that described by Simpson
 181 et al. (2019) (monthly-varying 3D-heating rates above 100 hPa derived from a double
 182 call to the radiation scheme with and without the aerosols). The amount of solar dim-
 183 ming needed is then calculated independently from the 3 × 3 SD ensemble, thus tak-
 184 ing into account changes in surface temperatures produced by the stratospheric heat-
 185 ing (see Fig. S1 and Simpson et al. (2019)). While Simpson et al. (2019) imposed heat-
 186 ing that was the same for the entire period, derived from the 2075–2095 period of aerosol
 187 injections, in our case the overall magnitude of the heating evolves year-by-year in the
 188 same way as the stratospheric heating in the 3 × 3 SS simulations. This is done in or-
 189 der to have both a more ‘self-consistent’ perturbation year after year and still realisti-
 190 cally evolving in magnitude as if the aerosol burden was increased every year. A com-
 191 parison of the different physical processes that can be investigated by comparing the dif-
 192 ferent sets of simulations is described in Fig. 1.

193 All analyses in this manuscript are for the period 2070–2089, as that 20-year time
 194 period has the greatest forcing of all periods simulated and thus the highest signal-to-
 195 noise ratio (MacMartin et al., 2019). The SS simulations are started in 2020. The SD
 196 simulations are branched off the SS simulations in 2060, substituting the injection of SO₂
 197 with solar reduction (as in Visioni, MacMartin, Kravitz, Richter, et al. (2020)). The first
 198 10 years are left out of the analyses to give the system time to relax to the new state,
 199 even though all stratospheric aerosols are already removed after the first 2 years with-

Figure 1. Summary of the simulations employed in this work. The white boxes give the name of these simulations as referred to in this paper and the size of the ensemble, in brackets. The orange boxes represent the key scientific questions that can be answered by comparing different sets of simulations.

Table 2. Summary of the main results of the five simulations, as departures from the 2010-2030 period in Control: T0, T1 and T0 represent the projections of near-surface air temperatures in the first three Legendre polynomial in K; Precipitation (P) and Precipitation-Evapotranspiration over land ($\Delta P - E_{land}$) in mm/day. Arctic September Sea ice (SSI) in $10^6 \times \text{km}^2$.

Simulation	ΔT_0	ΔT_1	ΔT_2	ΔP	$\Delta P - E_{land}$	ΔSSI
1 × 1 SD	-0.04	0.29	0.18	-0.09	-0.035	-1.1
1 × 1 SS	0.17	0.07	0.23	-0.14	-0.044	0.7
3 × 3 SD	-0.03	0.02	-0.02	-0.07	-0.041	2.7
3 × 3 SS	0.06	0.04	0.09	-0.12	-0.038	1.5
3 × 3 SDH	-0.10	0.02	-0.02	-0.10	-0.050	2.9

out injection. All simulations are compared against the period 2010-2030 (using the entire 20-member ensemble), termed Control in this work.

3 Results

All model simulations restore global surface temperature to within 0.17 K of the average in the Control period. In the period 2070-2089 considered in our analyses, that equates to an average cooling of 3.9K (Tilmes, Richter, Kravitz, et al., 2018) in order to maintain the same temperature as the period 2010-2030. The obtained AOD and solar dimming required to achieve the temperature goals are shown in Fig 2. There are clear differences in the solar dimming patterns that preview some of the observed changes that will be discussed later on. The uniform dimming in the 1×1 SD case implies an overcooling of the tropics and an undercooling at high latitudes (Govindasamy et al., 2003; Kravitz, Caldeira, et al., 2013), resulting in a reduction, for instance, in September sea ice in the Arctic (Table 2) even when global surface temperatures are restored. There are also evident differences with the 1×1 SS case, where the AOD produced by equatorial injections is not latitudinally uniform due to the tropical confinement of the aerosols (Visioni, Pitari, Tuccella, & Curci, 2018), amplifying even more the tropical overcooling. The increasing fractional solar reduction at higher latitudes compensates for this in the 3×3 cases, either by directly reducing sunlight or by injecting outside the tropics. Over 60° of latitude, however, the 3×3 SS differs further from the SD case due to the dynamical transport barrier there (Visioni, MacMartin, Kravitz, Lee, et al., 2020). Roughly, an AOD of 0.1 equates to a reduction of 1% in incoming solar irradiance (e.g. Hansen et al., 2005). In the 3×3 cases, SDH requires more solar reduction compared to SD. This is due to an increase in stratospheric water vapor resulting from tropopause warming (Visioni, Pitari, & Aquila, 2017; Tilmes, Richter, Mills, et al., 2018) as we show in Fig. S1, that in turn warms the surface (Hansen et al., 2005; Simpson et al., 2019).

3.1 Comparison of simulated surface temperatures and precipitation

In Fig. 3 we show the annually averaged surface temperature response in all cases relative to Control. Despite global mean temperature being within 0.17 K of the objec-

Figure 2. Comparison of stratospheric sulfate AOD obtained through SO₂ injections (SS) or solar dimming (SD) for the five simulations, both averaged over 2070-2089. In panel a), cases maintaining global mean temperature are shown. In panel b), cases maintaining global mean temperature, inter-hemispheric temperature gradient, and equator-to-pole temperature gradient are shown. AOD annual averages are shown in solid black, while solar dimming (expressed as a fraction of incoming solar radiation reduced $\times 10$) is shown in dashed black. Monthly AOD is shown with solid colors (see colorbar). In panel b), the dash-dotted line shows the solar dimming necessary for the SDH simulations. SO₂ injection latitudes are indicated by thin dashed lines.

Figure 3. Surface temperature changes for all simulations for 2070-2089 relative to 2010-2030. In the third column, areas are highlighted where surface temperature shows statistically significant (using a two-sided t-test with $p < 0.05$) changes between the simulations with SD and SS. Grey areas indicate regions in all maps where the differences are not statistically different from zero. Differences between the left and right maps are shown in Fig. S2

228
229
230
231
232
233
234
235
tive, local differences of up to 1–2 K are present; however, these differences are much smaller than those due to RCP 8.5 alone. The comparison of the 1×1 SD with both SS simulations highlights that, aside from a few features, simply turning down the sun is not a good analogue for how regional temperatures would respond to the stratospheric aerosols. Exceptions include the sign of the tropical overcooling and high-latitude under-cooling and the warming over the northern Atlantic Ocean (due to over-compensating the GHG-driven slowing down of the Atlantic Meridional Overturning Circulation (AMOC) in this model (Fasullo et al., 2018)).

236
237
238
239
240
241
242
243
244
245
246
247
248
249
250
251
These differences are due to various factors. For the 1×1 cases, as shown in Table 2, the magnitude of T1 and T2 in the SS case are not captured correctly by the SD case due to the peak in AOD in the tropics that does not resemble the uniform dimming in solar radiation (Fig. 2a). (Equatorial injection in this model results in slightly higher AOD in the northern hemisphere than the southern, roughly compensating T1 even though that was not an objective of the 1×1 SS simulation.) For the 3×3 cases this effect is less pronounced, since the injection locations are chosen so as to have a similar profile to the one actually achieved by the solar dimming (MacMartin et al., 2017). At very high latitudes in both hemispheres, however, some differences are present mostly due to the polar transport barriers (Visioni, MacMartin, Kravitz, Lee, et al., 2020) that reduce the high-latitude AOD. It is likely that a more uniform AOD distribution using more latitudes of injection (see for instance Dai et al., 2018) could produce results more closely resembling those from 1×1 SD: however, some differences would still remain due to the considerable variation across different months of the AOD (Fig. 2) compared to the constant dimming produced by the SD cases: as shown by Visoni, MacMartin, Kravitz, Richter, et al. (2020), seasonal variations in AOD can result in notably different surface climates.

252
253
254
255
256
257
258
259
260
Lastly, the other difference between the simulations is the lack of stratospheric heating in the SD simulations. Previous papers point to the substantial lower troposphere warming in the winter (relative to baseline) over the continental northern high latitudes (Europe and Asia), (Simpson et al., 2019; Jiang et al., 2019), and consistent with what has been postulated in the past literature on the Pinatubo 1991 eruption (Robock & Mao, 1995; Robock, 2000), link this at least in part to the stratospheric heating produced by the aerosols. A recent paper by Polvani et al. (2019) has however cast doubts on the physical causal link relating the two, showing that in large ensembles of simulations (one of them performed with WACCM4, a model similar to that used for the simulations in this

Figure 4. a) Seasonal cycle of surface temperatures over high northern latitudes for each ensemble (thick lines, see legend) and single ensemble members (thin lines of the same color). b) Same as a), but showing the anomaly compared to the annual mean and the shaded curves representing the ensemble variability as ± 1 standard error.

study) the winter warming over Eurasia does not appear to be a consistent result, being limited to only some members of the ensemble.

Jiang et al. (2019) suggest that shifts in the high-latitude seasonal cycle are partly due to the dynamic effects from the stratospheric heating and partly due to there being more sunlight to reflect in summer than winter, but were unable to quantify the breakdown of the relative importance of these. There they used, however, simulations with a stratospheric heating imposed on top of a 2010–2030 climate, and compared against a geoengineered climate at the end of the century. Here we have the opportunity to expand on previous analyses since we can directly compare simulations with similar temperature gradients and CO₂ concentrations, but different stratospheric responses. In Fig. 4a, we show the monthly temperatures over the selected area for all simulations: in this case, however, the locally enhanced warming over Eurasia is mixed with the different equator-to-pole temperature gradients (T2): for the 1×1 cases, the warming over high latitudes is primarily due to only keeping global mean temperature constant, which tends to overcool the tropics and undercool high latitudes (Ban-Weiss & Caldeira, 2010; Kravitz et al., 2019). This is further exacerbated in the case of SS since the AOD is mostly concentrated at tropical latitudes. As shown in Russotto and Ackerman (2018b) and Merlis and Henry (2018), the differences in energy transport due to differences in T2 also lead to a residual polar warming in simulations with uniform solar dimming. Therefore, isolating the contribution of residual warming in winter in particular to this high latitude annual-mean pattern requires looking at seasonal differences with respect to the annual mean (Fig. 4b, where we removed the annual mean temperature calculated in the same area in order to highlight just the seasonal variations) as in Jiang et al. (2019).

Thus we can see that the SD cases both have a moderate warming over DJF relative to the annual mean (0.75 K) whereas the others have a stronger winter warming (1.22K for 3×3 SS, 1.43K for 3×3 SDH, and 1.97K for 1×1 SS). The 1×1 SS and 3×3 SDH cases seem to have similar warming, and both have different warming than the 3×3 SS case. The differences between the 3×3 SS and SDH cases may be explained by looking at the seasonal differences in AOD: as discussed by Visioni, MacMartin, Kravitz, Lee, et al. (2020), for the 3×3 SS case, the high latitude AOD reaches a relative peak compared to the annual average exactly in the months where the winter warming is expected, while for the 1×1 SS case, the AOD results are much more uniform seasonally. From the comparison of the SD and SDH cases, we can observe that the winter warming observed over Eurasia in these simulations can only be partially explained by the stratospheric heating. Over half of the high latitude winter warming compared to the annual mean results from differences between SW and LW forcing which, as Govindasamy et al. (2003); Jiang et al. (2019) point out, is especially prominent at high latitudes, and that can't be avoided even if a more careful spatial distribution of the counteracting forcing is applied, as also suggested by Henry and Merlis (2020), who decomposed the vertical structure of the forcing in a single column model and found that inhomogeneities in the two forcings always result in some residual warming at high latitudes. To conclude, the observed differences between the analyzed simulations highlight a complex interplay of factors: the stratospheric heating directly affecting the surface climate through a modification of the North Atlantic Oscillation (Banerjee et al., 2020), the seasonality of the aerosol distribution (that in turn may be dynamically affected by the strengthening of the polar vortex, Visioni, MacMartin, Kravitz, Lee, et al. (2020)) and a fundamental dif-

Figure 5. Precipitation changes for all simulations for 2070-2089 relative to 2010-2030. In the third column, areas are highlighted where surface precipitation shows statistically significant (using a two-sided t-test with $p < 0.05$) changes between the simulations with SD and SS. Grey areas indicate regions in all maps where the differences are not statistically different from zero. Differences between the left and right maps are shown in Fig. S3

307
308
309
310
ference between the LW and SW radiative forcings; all of these factors indicate that, when assessing the projected potential of stratospheric sulfate geoengineering to mitigate changes in high-latitude ecosystems with the potential to release considerable amounts of carbon (Chen et al., 2020), the inclusion of realistic aerosol behavior is crucial.

311
312
313
314
315
316
In Fig. 5 we show the same comparison as in Fig. 3 but for total precipitation. Results for P-E (precipitation minus evapotranspiration) are reported in the supplementary material (Fig. S2). Generally, it is clear that even given the same temperature targets, there are substantial differences in the projected precipitation changes. In particular, both SD cases show reduced changes compared to the SS cases. Unlike for temperature, however, in this case the SDH case shows further similarities with 3×3 SS.

317
318
319
320
321
322
323
324
On a decadal scale, precipitation changes can be described by changes in total column energy, which can be broken up into column-integrated diabatic cooling and dry static energy flux divergence (Muller & O'Gorman, 2011). Kravitz, Rasch, et al. (2013) used this framework to explain a simulation analogous to 1×1 SD, and we adapt that method for the present study to explain the changes in Fig. 5, with the caveat that our period of analyses is not in a perfect steady state. Following the analyses in Kravitz, Rasch, et al. (2013), the differences in the column-integrated diabatic cooling (excluding latent heating), can be calculated as

$$\Delta Q = \Delta RF_{sfc} - \Delta RF_{TOA} - \Delta SH \quad (1)$$

325
326
327
328
where ΔRF_{sfc} is the net radiative flux at the surface (SW + LW; positive downward), ΔRF_{TOA} is the net radiative flux at the top-of-atmosphere (positive downward), and ΔSH is the change in sensible heat flux (positive upward, as is customary for turbulent fluxes).

329
Changes in precipitation can then be calculated as

$$L_c \Delta P = \Delta Q + \Delta H \quad (2)$$

330
331
332
333
334
335
336
337
338
339
340
341
342
343
344
345
346
where L_c is the latent heat of condensation, ΔQ is the column integrated diabatic cooling, and ΔH is the dry static energy flux divergence (calculated as a residual). In Fig. 6a-c we show that the SD and 3×3 SS experiments have very different column energy budgets that can help explain some of the differences in surface precipitation shown in Fig. 5. The comparison between panels 6a and 6b indicates that a part of the changes in ΔQ are co-located with differences in temperature between the 1×1 and 3×3 cases, especially in the tropical regions, where a uniform solar reduction (or equatorial stratospheric aerosol injections) tends to overcool the tropics and shifts the inter-tropical convergence zone location. Comparing the results with those for the SDH simulation indicates that part of the precipitation differences between SD and SS simulations can be reduced if the stratospheric heating term is included in the model simulations, due to a more realistic partition of energy in the column. Not all differences can be reduced this way: in Fig. 6d we show that differences in the energy flux divergence term are quite similar between the SD and SDH simulations, implying that some of the observed local changes are due to other processes. For instance, the seasonal dependence of AOD has been shown to affect precipitation regionally and seasonally (i.e. in the case of the monsoon season, or over Amazonia, Visioni, MacMartin, Kravitz, Richter, et al., 2020). This can be

Figure 6. Differences in the column-integrated diabatic cooling (ΔQ , W/m^2) between the $3 \times 3\text{SS}$ case and the three SD experiments (panels a,b and c, 2070-2089 average). d) Zonal and annual mean differences in the dry static energy flux divergence (ΔH , W/m^2) between the $3 \times 3\text{SS}$ case and the three SD experiments. See Fig.S7 for a comparison of zonal mean precipitation (in W/m^2) and ΔQ .

347 observed in Fig. S5 and S6, where we show the precipitation changes in two of the sea-
 348 sons (DJF and JJA). As an example, over India the magnitude of precipitation changes
 349 in JJA is larger in the 3×3 SS simulations than in other seasons, compared to SD and
 350 SDH: in this case, differences in cooling over the Tibetan plateau, driven by the seasonal
 351 variation of the AOD, would affect the monsoonal circulation, combined with energetic
 352 changes in the column produced by the stratospheric heating (Simpson et al., 2018; Vi-
 353 sioni, MacMartin, Kravitz, Richter, et al., 2020).

354 3.2 Solar dimming as a modeling analogue for sulfate injections

355 From our analyses, it is clear that generally the outcomes of SD simulations and
 356 SS simulations are different: in this section, we try to better quantify these differences
 357 to better answer the initial question: is solar dimming a good proxy for stratospheric sul-
 358 fate geoengineering? As a baseline for comparison, we use our 20 (members) $\times 20$ (years)
 359 3×3 SS simulations as our best estimate of the forced response (in this model) of an
 360 SS strategy that aims to minimize changes in surface climate, and we compare this with
 361 the other four simulations (3 members $\times 20$ years for $1 \times 1\text{SD}$, $1 \times 1\text{SS}$, $3 \times 3\text{SD}$ and
 362 $3 \times 3\text{DH}$). The metrics we use are surface temperature, precipitation, precipitation mi-
 363 nus evapotranspiration, monthly maximum temperatures and monthly maximum pre-
 364 cipitation, which have been used previously to define the impacts of geoengineering (P. Irvine
 365 et al., 2019), plotted on Taylor diagrams (Fig 7, Taylor, 2001). These kind of diagrams
 366 are generally used to evaluate multiple model performances compared to observations
 367 on three metrics: the Pearson correlation coefficient, plotted as the azimuthal angle, mea-
 368 sures the pattern similarities; the root mean squared error (RMSE), proportional to the
 369 distance from the point on the x-axis defined as our benchmark, measures the overall dif-
 370 ference between that benchmark and the other simulations; and the standard deviation
 371 σ , as distance from the axis origin, that measures the amplitude of the variations in both
 372 simulated and the benchmark values (that lie on the dashed line). The similarity is then
 373 evaluated as the distance between the single value for each simulation and the bench-
 374 mark value that lies on the x-axis. In Fig 7 we also include gray shading that serves as
 375 a measure of the differences induced by the natural variability. To construct this met-
 376 ric, we consider the general difference between any random pick of 3 ensemble members
 377 of $3 \times 3\text{SS}$ simulations (overall, $\binom{20}{3} = 1140$) and plot each of the resulting sub-sets against
 378 the full 20 -member ensemble (the operation performed to obtain this is shown in Fig.
 379 S8). The grey shading can therefore be considered as the effect of sampling a smaller en-
 380 semble size: if one of the other simulations approaches this area, we cannot tell whether
 381 the residual difference is due to natural variability or differences in physical processes
 382 between the simulations. From the results in Fig. 7, we conclude that simply turning down
 383 the sun produces regional climate results that are highly uncorrelated from those obtained
 384 in 3×3 SS simulations. The 3×3 SDH simulation is most similar to the baseline indi-
 385 cating the importance of (1) tailoring the pattern of solar dimming so that the net ef-
 386 fect matches the radiative forcing of the aerosols, and (2) including stratospheric heat-
 387 ing that would result from the aerosols. This result especially holds for hydrological quan-
 388 tities, indicating that the stratospheric changes produced as a response to stratospheric
 389 heating are an especially important component of the climate response to stratospheric
 390 sulfate aerosols. For temperature, the differences between 3×3 SD and 3×3 SDH are

Figure 7. Taylor diagrams for various simulated quantities as compared to the 3×3 SS case. The shaded areas indicate differences indistinguishable from natural variability between a given ensemble and the 3×3 SS ensemble. See text and Fig. S8 for further description.

more marginal, indicating that differences from baseline are predominantly due to the pattern of forcing (see Fig. 2).

3.3 Simulation of other surface variables

Taylor diagrams are most effective for quantities that present at least some patterns of similarity to the baseline. There are other quantities where this does not hold, for example incoming solar radiation at the surface, where previous studies looking at ecologically-relevant metrics (Dagon & Schrag, 2019) have used solar dimming simulations to predict vegetation changes under geoengineering. In Fig. 8 we show some of the differences between SD and SS in 14 locations around the globe (the specific locations are shown in Fig. S9: only changes over land are considered in these analyses). We have chosen these locations as some of the largest biomass regions in the world: large forest (Song et al., 2018) in all continents save Antarctica, and the US Corn-belt (Green et al., 2018). We first consider the overall amount of incoming solar radiation at the surface in these zones, and find that differences attributable to both the objectives (1×1 and 3×3) and strategies (SD and SS). In some places, counter-intuitively, the overall amount of incoming solar radiation even goes up compared to the control period, mainly due to local changes in cloud coverage (Fig. 9). Differences between SD and SS simulations in this case are associated with very high clouds, and results would be rather different if we consider low-, medium- or high-altitude clouds (see Figs. S10-S12), suggesting different mechanisms by which geoengineering, in these simulations, affects cloud coverage. In particular, while low-altitude clouds show very similar changes between SS and SD simulations, medium-altitude clouds present differences that are resolved (at mid and low latitudes) by including the stratospheric heating term, suggesting their modification is driven mostly by changes produced by the temperature anomalies in the lower stratosphere and not by climate-change driven factors (e.g. Norris et al., 2016). High-altitude ice clouds, that have a strong radiative effect on outgoing longwave radiation at mid-latitudes (Fusina et al., 2007), show the highest differences. Contrary to previous research (Kuebbeler et al., 2012; Visioni, Pitari, Di Genova, et al., 2018) with different models that showed how these changes are also driven by the vertical temperature gradient, here the main cause of the changes seems to be the aerosols themselves. While it has already been suggested that this might be due to incorrect parametrizations in CESM1(WACCM) (Schmidt et al., 2018), further investigation is warranted.

Similarly, large differences are present when considering the changes in the ratio of direct incoming solar radiation compared to the total: the portion of sunlight arriving directly, versus that arriving diffused might be very important when considering the effects on different kinds of vegetation and ecosystems (Gu et al., 2003; Mercado et al., 2009): in this case (Fig. 8b) large differences are not only present between SS and SD cases, but even among different strategies for similar methods (e.g., differences between 1×1 SS and 3×3 SS). For the 3×3 SD and 3×3 SHD experiments, changes in this ratio are very small, as the changes in cloud coverage are also mostly negligible in large parts of the planet (Fig. 9) for these experiments. On the other hand in the 1×1 SD experiment, the model projects a small increase in direct incoming solar radiation in most areas, due to the more significant decrease in cloud coverage over most of the considered areas. Similarly, in the SS experiments the presence of the aerosols reduces the amount of direct incoming solar radiation due to scattering from the aerosols themselves, but the magnitude of these changes is remarkably different: this is due both to a different distribution of the aerosols (see Fig. 2 and Kravitz et al. (2019)), that are much higher in

Figure 8. a) Changes in incoming solar radiation over land in 14 locations with some of the largest forests (see Fig. S9 and text) for all five experiments in the period 2070-2089 compared to 2010-2030 in RCP8.5. b) Changes in the portion of incoming solar radiation over land arriving directly as a fraction of the total incoming solar radiation for all five experiments in the period 2070-2089 compared to 2010-2030 in RCP8.5. c) Simulated changes in Total Leaf Area Index in those locations for all five experiments compared to the 2070-2089 period in RCP8.5.

Figure 9. Simulated total cloud fraction differences (dimensionless) in the 5 geoengineering experiment against the Control 2010-2030 period. Grey areas indicate regions in all maps where the differences are not statistically different from zero (using a two-sided t-test with $p < 0.05$).

the 1×1 SS experiment at low latitudes and to a difference in the simulated cloud response, as 1×1 SS predicts a larger increase in medium-altitude clouds compared to 3×3 SS (Fig. S11). An example of how changes in radiation could affect our understanding of the impacts of geoengineering is given in Fig. 8c, where changes in Leaf Area Index (LAI) are shown against the same time period (2079-2089) in RCP8.5 (to account for changes in LAI produced by increasing CO₂ concentrations, that are the main driver of LAI changes, unlike the first two panels). LAI is determined dynamically in the land model in CESM, and responds to changes in temperature and hydrology together with changes in photosynthesis and respiration dependant on the incoming solar radiation. For this reason the various experiments project different vegetation responses depending on the geoengineering strategy, sometimes also with different sign: for instance in the Congo Basin, the SS experiments project a modest increase in LAI compared to RCP8.5 while the SD experiments project a large decrease (especially for the 1×1 case). Overall, it is hard to directly link the changes in LAI in the interactive land model simply to the changes in incoming solar radiation, given the contribution of other factors, such as the CO₂ increase, different regional temperatures and changes in their seasonal cycle, precipitation and more, and given the feedback of these changes themselves on some of those factors (for instance, the link of plant transpiration and local hydrology). But in light of the importance of understanding ecosystem changes in the context of stratospheric sulfate geoengineering, this suggests that future studies aiming to do such assessments should take great care to use simulations where the aerosols are present in a realistic distribution.

A correct representation of the changes in cloudiness would be important not just for the radiation effects on ecosystems: the importance of clouds in the surface radiative budget of continental ice sheets (McIlholland et al., 2017; van Kampenhout et al., 2020) indicates that, in order to assess the ability of SG to limit sea level rise (P. J. Irvine et al., 2018) and restore continental glaciers extent, solar dimming simulations as a proxy might produce incorrect results by incorrectly reproducing cloud changes and, partially, high-latitudinal warming produced by the stratospheric heating.

3.4 Simulation of the stratospheric response

As we've shown in the previous sections, the stratospheric response is an important component in correctly capturing the climate response to sulfate injections. In the case of some surface variables, this happens because of dynamical changes in the circulation (Fig. S13). Previous works have shown that stratospheric chemistry would also be impacted by the sulfate aerosols (Visioni, Pitari, Aquila, Tilmes, et al., 2017; Tilmes, Richter, Mills, et al., 2018; Vattioni et al., 2019) but in most cases, these changes (such as in the concentration of N₂O and CH₄) are also due to modifications of stratospheric

Figure 10. Changes in stratospheric ozone concentrations (ppm) compared to the same period (2070-2089) in RCP8.5. Average tropopause height for RCP8.5 (continuous black line) and the geoengineering simulations in the panels (dashed black line) are also shown. Hatched areas indicate regions in all maps where the differences are not statistically different from zero (using a two-sided t-test with $p < 0.05$).

475 dynamics. The effects of SS on stratospheric ozone may however vary due to different
476 causes other than dynamical changes (Tilmes et al., 2008; Pitari et al., 2014; Tilmes, Richter,
477 Mills, et al., 2018), for instance by the direct increase in Surface Area Density (SAD)
478 resulting in changes in heterogeneous chemistry (Richter et al., 2017), both in the trop-
479 ics and at higher altitudes. These changes might be important to project changes in sur-
480 face UV (Madronich et al., 2018), with consequent human impacts (Eastham et al., 2018).

481 Chemical ozone destruction due to increased SAD, especially in the polar regions,
482 is mostly tied to changes in ozone-depleting substances (Morgenstern et al., 2018) that
483 are projected to strongly decrease in the coming decades (Dhomse et al., 2018). There-
484 fore, the relative contributions of chemical versus dynamical ozone destruction depend
485 on the decade of analyses. In our analyses towards the end of the century, the predom-
486 inant effect in the tropical regions in the mid-stratosphere is driven by dynamical cir-
487 culation changes, as can be observed in the comparison between Fig. 10c and 10e, ad-
488 vecting ozone-poor air from lower to higher altitudes due to an increase in vertical ve-
489 locities and an acceleration of the Brewer-Dobson circulation and by an increase in strato-
490 spheric water vapor that modifies the HO_x cycle-mediated ozone loss (Richter et al., 2017;
491 Tilmes, Richter, Mills, et al., 2018). At high-latitudes, on the other hand, the SAD-induced
492 changes result in a delay of the predicted recovery under baseline conditions (as discussed
493 in Tilmes et al., 2008) that is not observed in the SDH case in Fig. 10e.

4 Conclusions

Simulations with climate models are our main instrument for understanding the possible changes to the Earth System that would be produced by using geoengineering to counteract the effects of increases in GHGs. Properly simulating the projected regional effects is crucial in order to inform policy-makers and the general population about the possible outcomes.

Even without considering geoengineering, there are uncertainties in the projected local changes under climate change, although with improvements in climate models, these uncertainties are decreasing (Christensen et al., 2007; Matte et al., 2019). For solar geoengineering, our assessment of local changes does however depend on more factors than for climate change: aside from the uncertainty in specific physical processes (Kravitz & MacMartin, 2020), these factors include i) the desired level of cooling (P. Irvine et al., 2019; MacMartin et al., 2019; Tilmes et al., 2020); ii) the specific technique simulated (i.e. the method chosen to reduce surface temperatures, Niemeier et al., 2013; Gasparini et al., 2020), and iii) within the same technique, the specific strategy deployed (Kravitz et al., 2019; Visoni, MacMartin, Kravitz, Richter, et al., 2020). There is thus a compound of different kinds of uncertainties (those listed, and those we don't know we don't know about) that result in challenges in clearly determining - and communicating - what effects geoengineering would have locally.

This is made even more challenging if the term “solar geoengineering” is used improperly to conflate different things, and in particular, stratospheric sulfate injections in all its forms and a global reduction in the incoming solar radiation (i.e. the G1 experiment described in Kravitz et al., 2011). On one hand, the use of the latter to simplify the former is understandable, considering the challenges in correctly simulating stratospheric dynamics and stratospheric sulfate interactions (Timmreck et al., 2018; Kravitz & MacMartin, 2020). In this work we have shown, however, that the climate outcomes in the two cases present large difference. In this work we have focused on analyzing some of the key variables often used to evaluate climate engineering projections: surface temperatures, the hydrological cycle, minimum and maximum yearly temperatures, stratospheric ozone, clouds and incoming solar radiation at the surface. In particular, we have shown that while both methods can reduce globally averaged surface temperatures and other globally-defined climate metrics, depending on the method and on the choices of targets large regional differences are observable in the annually averaged surface temperatures. Partially these differences can be reduced if the reduction in the solar constant is performed in a way as to more closely resemble the shape of the stratospheric optical depth resulting from the sulfate injections, but we show that in high-latitudinal regions the effect of the stratospheric heating is a contributor to the surface response. The effect of the stratospheric heating is even more evident for precipitation changes, due to its contribution to the partitioning of the energy budget in the vertical column. For other variables that might be relevant for a comprehensive assessment of the effects of sulfate geoengineering on ecosystems, such as the changes in diffuse radiation at the surface, the overall effect is tied to both the actual presence of the aerosols and to the changes in cloud coverage that, at least in this model, appear to be sensitive to the different temperature gradients, to the stratospheric heating and to the aerosols themselves: for this reason, simulations that do not include the physical response of the aerosols might not be suitable for impact assessments.

Overall, our results confirm and strengthen previous observations related to the changes that would be produced by the presence of stratospheric aerosols, and highlight the need to include these processes whenever the surface impacts of sulfate geoengineering are to be determined. We can summarize the main differences between a top-of-the-atmosphere solar constant reduction and the presence stratospheric aerosols by identifying three mechanisms that largely explain those differences:

Figure 11. Infographic of the most important studied effects produced by solar geoengineering on the various components of the climate system. The three different ways in which climate models can simulate the effects of the injection of stratospheric sulfate are shown on top, going from the least to the most complex representation: solar dimming, adding the stratospheric heating on top of the solar dimming or directly simulating the aerosols. All three are then connected to the effect of their presence on various components of the Earth System (divided in atmospheric dynamics, atmospheric chemistry, radiative fluxes and direct surface effects) through arrows that highlight some of the important interactions (recognizing that ultimately, everything is influenced by everything else).

- 546 1. the aerosols do not produce a uniform reduction in the incoming solar radiation
 547 (both latitudinally and temporally, Fig. 2). Especially if the deployed injection
 548 strategy has particular goals resulting in a particular aerosol distribution (e.g., the
 549 strategy described in Tilmes, Richter, Kravitz, et al., 2018), the comparison with
 550 a uniform solar dimming produces widely different results, both in regional tem-
 551 peratures and precipitations. This is mainly due to differences in the resulting tem-
 552 perature gradients, that produce shifts in the climate response (as discussed, for
 553 different SS strategies, in Kravitz et al. (2019)). Because of this, these discrep-
 554 ances can be reduced if the solar constant is dimmed not uniformly, but in a way
 555 resembling the distribution of the simulated aerosols, in order to have the same
 556 temperature gradients that SS experiment is designed to maintain.
- 557 2. the aerosols produce a localized stratospheric warming that results in various changes
 558 at the surface and in the upper atmosphere. Even if the same surface tempera-
 559 ture gradients are maintained between experiments, quantities such as precipita-
 560 tion and P-E still show differences when the sun is dimmed compared to when the
 561 aerosols are simulated. In our simulations, combining solar dimming with strato-
 562 spheric heating helps further reduce the differences with the 3×3 SS strategy.
- 563 3. the aerosols scatter part of the incoming sunlight, modifying the ratio of direct
 564 to diffuse radiation, possibly modifying the projected changes on vegetation and
 565 evapotranspiration. Stratospheric aerosols affect stratospheric chemistry (princi-
 566 pally ozone), and also ultimately result in the deposition of sulfate at the surface
 567 that might have environmental effects (albeit those have been projected to be small,
 568 see Kravitz et al., 2009; Visioni, Slessarev, et al., 2020).

569 These points are summarized in Fig. 11, highlighting both the causes of the sim-
 570 ultated changes and the interconnections in the climate system that result in changes at
 571 the surface; in the figure, we also include effects not directly analyzed in this paper but
 572 discussed in referenced works.

573 Are the produced changes in the surface climate significant? This is a question that
 574 depends on the amount of cooling provided by the geoengineering and thus on the amount
 575 of injected SO_2 . In the simulations analyzed here, we use the RCP8.5 scenario, that has
 576 very high emissions throughout all the century and that result in around 4 degrees of
 577 warming in the 2070-2089 period. This can therefore be considered an ‘extreme’ scenario,
 578 resulting in the need of very high injection amounts producing a considerable perturba-
 579 tion in stratospheric temperature. Considering a peak-shaving scenario where a limited
 580 deployment is aimed at remaining below an otherwise dangerous temperature thresh-
 581 old (MacMartin & Kravitz, 2019; Tilmes et al., 2020) are projected to result, very likely,
 582 in some of these changes being indistinguishable from the normal climate variability (MacMartin
 583 et al., 2019).

In the last years, however, the topic of the impacts of climate engineering has gathered more and more interest not only from climate scientists but also from the broader scientific community, interested in impacts both on human activities (Tavoni et al., 2017) and on the environment and ecosystems. Because of this, a proper, robust assessment of all possible side effects is becoming crucial. While this mainly requires tackling uncertainties in our physical knowledge and shortcomings in our climate simulations (Kravitz & MacMartin, 2020), the importance of recognizing the shortcomings of using solar dimming as a proxy for stratospheric sulfate geoengineering can't be ignored.

Acknowledgments

The authors would like to thank I.R. Simpson for the numerous meaningful discussions and I.R. Simpson and S. Tilmes for their support with the CESM1(WACCM) simulations. We would like to acknowledge high-performance computing support from Cheyenne (<https://doi.org/10.5065/D6RX99HX>) provided by NCAR's Computational and Information Systems Laboratory, sponsored by the National Science Foundation. Support for D. V. and D. G. M. was provided by the Atkinson Center for a Sustainable Future at Cornell University and by the National Science Foundation through agreement CBET-1818759. Support for B.K. was provided in part by the National Science Foundation through agreement CBET-1931641, the Indiana University Environmental Resilience Institute, and the *Prepared for Environmental Change* Grand Challenge initiative. The Pacific Northwest National Laboratory is operated for the US Department of Energy by Battelle Memorial Institute under contract DE-AC05-76RL01830. Data from the simulations used in this work is available at <https://doi.org/10.5065/D6JH3JXX> (for the 3×3SS, 1×1SS and RCP8.5 simulations) and <https://doi.org/10.7298/z8c9-3p43> (for all other simulations).

References

- Aquila, V., Garfinkel, C., Newman, P., Oman, L., & Waugh, D. (2014). Modifications of the quasi-biennial oscillation by a geoengineering perturbation of the stratospheric aerosol layer. *Geophysical Research Letters*, 41(5), 1738–1744.
- Banerjee, A., Butler, A. H., Polvani, L. M., Robock, A., Simpson, I. R., & Sun, L. (2020). Robust winter warming over eurasia under stratospheric sulfate geoengineering – the role of stratospheric dynamics. *Atmospheric Chemistry and Physics Discussions*, 2020, 1–20. Retrieved from <https://acp.copernicus.org/preprints/acp-2020-965/> doi: 10.5194/acp-2020-965
- Ban-Weiss, G. A., & Caldeira, K. (2010). Geoengineering as an optimization problem. *Environmental Research Letters*, 5(3). doi: 10.1088/1748-9326/5/3/034009
- Budyko, M. I. (1978). *The climate of the future*. American Geophysical Union. Retrieved from <http://dx.doi.org/10.1002/9781118665251.ch7> doi: 10.1002/9781118665251.ch7
- Chen, Y., Liu, A., & Moore, J. C. (2020). Mitigation of arctic permafrost carbon loss through stratospheric aerosol geoengineering. *Nature Communications*, 11(1), 2430. Retrieved from <https://doi.org/10.1038/s41467-020-16357-8> doi: 10.1038/s41467-020-16357-8
- Cheng, W., MacMartin, D. G., Dagon, K., Kravitz, B., Tilmes, S., Richter, J. H., ... Simpson, I. R. (2019). Soil moisture and other hydrological changes in a stratospheric aerosol geoengineering large ensemble. *Journal of Geophysical Research: Atmospheres*, 124(23), 12773–12793. Retrieved from <https://agupubs.onlinelibrary.wiley.com/doi/abs/10.1029/2018JD030237> doi: 10.1029/2018JD030237
- Christensen, J. H., Hewitson, B., Busuioc, A., Chen, A., Gao, X., Held, R., ... others (2007). Regional climate projections. In *Climate Change, 2007: The*

- Physical Science Basis. Contribution of Working group I to the Fourth Assessment Report of the Intergovernmental Panel on Climate Change, University Press, Cambridge, Chapter 11* (pp. 847–940).

Crutzen, P. J. (2006). Albedo enhancement by stratospheric sulfur injections: A contribution to resolve a policy dilemma? *Climatic Change*, 77(3), 211–220. Retrieved from <http://dx.doi.org/10.1007/s10584-006-9101-y> doi: 10.1007/s10584-006-9101-y

Dagon, K., & Schrag, D. P. (2019). Quantifying the effects of solar geoengineering on vegetation. *Climatic Change*, 153(1), 235–251.

Dai, Z., Weisenstein, D. K., & Keith, D. W. (2018). Tailoring Meridional and Seasonal Radiative Forcing by Sulfate Aerosol Solar Geoengineering. *Geophysical Research Letters*, 45(2), 1030–1039. doi: 10.1002/2017GL076472

Danabasoglu, G., Bates, S. C., Briegleb, B. P., Jayne, S. R., Jochum, M., Large, W. G., ... Yeager, S. G. (2012, 03). The CCSM4 Ocean Component. *Journal of Climate*, 25(5), 1361–1389. Retrieved from <https://doi.org/10.1175/JCLI-D-11-00091.1> doi: 10.1175/JCLI-D-11-00091.1

Dhomse, S. S., Kinnison, D., Chipperfield, M. P., Salawitch, R. J., Cionni, I., Hegglin, M. I., ... Zeng, G. (2018). Estimates of ozone return dates from Chemistry-Climate Model Initiative simulations. *Atmospheric Chemistry and Physics*, 18(11), 8409–8438. doi: 10.5194/acp-18-8409-2018

Eastham, S. D., Weisenstein, D. K., Keith, D. W., & Barrett, S. R. (2018). Quantifying the impact of sulfate geoengineering on mortality from air quality and UV-B exposure. *Atmospheric Environment*, 187, 424 – 434. Retrieved from <http://www.sciencedirect.com/science/article/pii/S1352231018303510> doi: <https://doi.org/10.1016/j.atmosenv.2018.05.047>

Fasullo, J. T., Simpson, I. R., Kravitz, B., Tilmes, S., Richter, J. H., MacMartin, D. G., & Mills, M. J. (2018). Persistent polar ocean warming in a strategically geoengineered climate. *Nature Geoscience*, 11(12), 910–914. Retrieved from <http://dx.doi.org/10.1038/s41561-018-0249-7> doi: 10.1038/s41561-018-0249-7

Ferraro, A. J., Charlton-Perez, A. J., & Highwood, E. J. (2015). Stratospheric dynamics and midlatitude jets under geoengineering with space mirrors and sulfate and titania aerosols. *Journal of Geophysical Research: Atmospheres*, 120(2), 414–429. Retrieved from <https://agupubs.onlinelibrary.wiley.com/doi/abs/10.1002/2014JD022734> doi: 10.1002/2014JD022734

Fusina, F., Spichtinger, P., & Lohmann, U. (2007). Impact of ice supersaturated regions and thin cirrus on radiation in the midlatitudes. *Journal of Geophysical Research: Atmospheres*, 112(D24), n/a–n/a. Retrieved from <http://dx.doi.org/10.1029/2007JD008449> (D24S14) doi: 10.1029/2007JD008449

Gasparini, B., McGraw, Z., Storelvmo, T., & Lohmann, U. (2020, apr). To what extent can cirrus cloud seeding counteract global warming? *Environmental Research Letters*, 15(5), 054002. Retrieved from <https://doi.org/10.1088/1748-9326%2Fab71a3> doi: 10.1088/1748-9326/ab71a3

Gienke, S., Irvine, P. J., & Lawrence, M. G. (2015). The impact of geoengineering on vegetation in experiment G1 of the GeoMIP. *Journal of Geophysical Research: Atmospheres*, 120(19), 10,196–10,213. Retrieved from <https://agupubs.onlinelibrary.wiley.com/doi/abs/10.1002/2015JD024202> doi: 10.1002/2015JD024202

Govindasamy, B., Caldeira, K., & Duffy, P. (2003). Geoengineering earth's radiation balance to mitigate climate change from a quadrupling of CO₂. *Global and Planetary Change*, 37(1), 157 - 168. Retrieved from <http://www.sciencedirect.com/science/article/pii/S0921818102001959> (Evaluation, Intercomparison and Application of Global Climate Models) doi: [https://doi.org/10.1016/S0921-8181\(02\)00195-9](https://doi.org/10.1016/S0921-8181(02)00195-9)

Green, T. R., Kipka, H., David, O., & McMaster, G. S. (2018). Where is the

- 690 USA Corn Belt, and how is it changing? *Science of The Total Environment*, 618, 1613 - 1618. Retrieved from <http://www.sciencedirect.com/science/article/pii/S0048969717326761> doi: <https://doi.org/10.1016/j.scitotenv.2017.09.325>
- 691 Gu, L., Baldocchi, D. D., Wofsy, S. C., Munger, J. W., Michalsky, J. J., Urbanski,
 692 S. P., & Boden, T. A. (2003). Response of a deciduous forest to the mount
 693 pinatubo eruption: Enhanced photosynthesis. *Science*, 299(5615), 2035–2038.
 Retrieved from <https://science.scienmag.org/content/299/5615/2035>
 doi: 10.1126/science.1078366
- 694 Guo, A., Moore, J. C., & Ji, D. (2018). Tropical atmospheric circulation response
 695 to the G1 sunshade geoengineering radiative forcing experiment. *Atmo-*
 696 *spheric Chemistry and Physics*, 18(12), 8689–8706. Retrieved from <https://www.atmos-chem-phys.net/18/8689/2018/> doi: 10.5194/acp-18-8689-2018
- 697 Hansen, J., Sato, M., Ruedy, R., Nazarenko, L., Lacis, A., Schmidt, G. A., ...
 698 Zhang, S. (2005). Efficacy of climate forcings. *Journal of Geophysical Research: Atmo-*
 699 *spheres*, 110(D18). Retrieved from <https://agupubs.onlinelibrary.wiley.com/doi/abs/10.1029/2005JD005776> doi: 10.1029/2005JD005776
- 700 Harding, A. R., Ricke, K., Heyen, D., MacMartin, D. G., & Moreno-Cruz, J.
 701 (2020). Climate econometric models indicate solar geoengineering would
 702 reduce inter-country income inequality. *Nature Communications*, 11(1),
 703 227. Retrieved from <https://doi.org/10.1038/s41467-019-13957-x> doi:
 704 10.1038/s41467-019-13957-x
- 705 Henry, M., & Merlis, T. M. (2020). Forcing dependence of atmospheric lapse rate
 706 changes dominates residual polar warming in solar radiation management
 707 climate scenarios. *Geophysical Research Letters*, 47(15), e2020GL087929.
 Retrieved from <https://agupubs.onlinelibrary.wiley.com/doi/abs/10.1029/2020GL087929> (e2020GL087929 10.1029/2020GL087929) doi:
 708 10.1029/2020GL087929
- 709 Irvine, P., Emanuel, K., He, J., Horowitz, L. W., Vecchi, G., & Keith, D. (2019).
 710 Halving warming with idealized solar geoengineering moderates key climate
 711 hazards. *Nature Climate Change*, 9(4), 295–299. Retrieved from <http://dx.doi.org/10.1038/s41558-019-0398-8> doi: 10.1038/s41558-019-0398-8
- 712 Irvine, P. J., & Keith, D. W. (2020, mar). Halving warming with stratospheric
 713 aerosol geoengineering moderates policy-relevant climate hazards. *Environmen-*
 714 *tal Research Letters*, 15(4), 044011. doi: 10.1088/1748-9326/ab76de
- 715 Irvine, P. J., Keith, D. W., & Moore, J. (2018). Brief communication: Under-
 716 standing solar geoengineering's potential to limit sea level rise requires at-
 717 tention from cryosphere experts. *The Cryosphere*, 12(7), 2501–2513. Re-
 718 tried from <https://tc.copernicus.org/articles/12/2501/2018/> doi:
 719 10.5194/tc-12-2501-2018
- 720 Ji, D., Fang, S., Curry, C. L., Kashimura, H., Watanabe, S., Cole, J. N. S., ...
 721 Moore, J. C. (2018). Extreme temperature and precipitation response to
 722 solar dimming and stratospheric aerosol geoengineering. *Atmospheric Chem-*723*
 724 *istry and Physics**, 18(14), 10133–10156. Retrieved from <https://www.atmos-chem-phys.net/18/10133/2018/> doi: 10.5194/acp-18-10133-2018
- 725 Jiang, J., Cao, L., MacMartin, D. G., Simpson, I. R., Kravitz, B., Cheng, W., ...
 726 Mills, M. J. (2019). Stratospheric Sulfate Aerosol Geoengineering Could Al-
 727 ter the High-Latitude Seasonal Cycle. *Geophysical Research Letters*, 46(23),
 728 14153–14163. doi: 10.1029/2019GL085758
- 729 Jones, A. C., Hawcroft, M. K., Haywood, J. M., Jones, A., Guo, X., & Moore,
 730 J. C. (2018). Regional Climate Impacts of Stabilizing Global Warming
 731 at 1.5 K Using Solar Geoengineering. *Earth's Future*, 6(2), 230–251. doi:
 732 10.1002/2017EF000720
- 733 Kalidindi, S., Bala, G., Modak, A., & Caldeira, K. (2015). Modeling of solar ra-
 734 diation management: a comparison of simulations using reduced solar con-

- stant and stratospheric sulphate aerosols. *Climate Dynamics*, 44(9), 2909–2925. Retrieved from <https://doi.org/10.1007/s00382-014-2240-3> doi: 10.1007/s00382-014-2240-3
- Kleinschmitt, C., Boucher, O., & Platt, U. (2018). Sensitivity of the radiative forcing by stratospheric sulfur geoengineering to the amount and strategy of the so₂ injection studied with the LMDZ-S3A model. *Atmospheric Chemistry and Physics*, 18(4), 2769–2786. Retrieved from <https://www.atmos-chem-phys.net/18/2769/2018/> doi: 10.5194/acp-18-2769-2018
- Kravitz, B., Caldeira, K., Boucher, O., Robock, A., Rasch, P. J., Alterskjær, K., ... Yoon, J.-H. (2013). Climate model response from the geoengineering model intercomparison project (geomip). *Journal of Geophysical Research: Atmospheres*, 118(15), 8320–8332. Retrieved from <https://agupubs.onlinelibrary.wiley.com/doi/abs/10.1002/jgrd.50646> doi: 10.1002/jgrd.50646
- Kravitz, B., Lamarque, J.-F., Tribbia, J. J., Tilmes, S., Vitt, F., Richter, J. H., ... Mills, M. J. (2017). First Simulations of Designing Stratospheric Sulfate Aerosol Geoengineering to Meet Multiple Simultaneous Climate Objectives. *Journal of Geophysical Research: Atmospheres*, 122(23), 12,616–12,634. doi: 10.1002/2017jd026874
- Kravitz, B., & MacMartin, D. G. (2020). Uncertainty and the basis for confidence in solar geoengineering research. *Nature Reviews Earth & Environment*, 1(1), 64–75. Retrieved from <http://dx.doi.org/10.1038/s43017-019-0004-7> doi: 10.1038/s43017-019-0004-7
- Kravitz, B., MacMartin, D. G., & Caldeira, K. (2012). Geoengineering: Whiter skies? *Geophysical Research Letters*, 39(11). Retrieved from <https://agupubs.onlinelibrary.wiley.com/doi/abs/10.1029/2012GL051652> doi: 10.1029/2012GL051652
- Kravitz, B., MacMartin, D. G., Tilmes, S., Richter, J. H., Mills, M. J., Cheng, W., ... Vitt, F. (2019). Comparing surface and stratospheric impacts of geoengineering with different SO₂ injection strategies. *Journal of Geophysical Research: Atmospheres*, 124(14), 7900–7918. Retrieved from <https://agupubs.onlinelibrary.wiley.com/doi/abs/10.1029/2019JD030329> doi: 10.1029/2019JD030329
- Kravitz, B., MacMartin, D. G., Wang, H., & Rasch, P. J. (2016). Geoengineering as a design problem. *Earth System Dynamics*, 7(2), 469–497. doi: 10.5194/esd-7-469-2016
- Kravitz, B., Rasch, P. J., Forster, P. M., Andrews, T., Cole, J. N., Irvine, P. J., ... Yoon, J. H. (2013). An energetic perspective on hydrological cycle changes in the Geoengineering Model Intercomparison Project. *Journal of Geophysical Research Atmospheres*, 118(23), 13,087–13,102. doi: 10.1002/2013JD020502
- Kravitz, B., Robock, A., Boucher, O., Schmidt, H., Taylor, K. E., Stenchikov, G., & Schulz, M. (2011). The Geoengineering Model Intercomparison Project (GeoMIP). *Atmospheric Science Letters*, 12(2), 162–167. Retrieved from <https://rmets.onlinelibrary.wiley.com/doi/abs/10.1002/asl.316> doi: 10.1002/asl.316
- Kravitz, B., Robock, A., Oman, L., Stenchikov, G., & Marquardt, A. B. (2009). Sulfuric acid deposition from stratospheric geoengineering with sulfate aerosols. *Journal of Geophysical Research Atmospheres*, 114(14), 1–7. doi: 10.1029/2009JD011918
- Kuebbeler, M., Lohmann, U., & Feichter, J. (2012). Effects of stratospheric sulfate aerosol geo-engineering on cirrus clouds. *Geophysical Research Letters*, 39(23). Retrieved from <http://dx.doi.org/10.1029/2012GL053797> (L23803) doi: 10.1029/2012GL053797
- Lee, W., MacMartin, D., Visioni, D., & Kravitz, B. (2020). Expanding the design

- space of stratospheric aerosol geoengineering to include precipitation-based objectives and explore trade-offs. *Earth System Dynamics Discussions*, 2020, 1–31. Retrieved from <https://esd.copernicus.org/preprints/esd-2020-58/> doi: 10.5194/esd-2020-58
- Low, S., & Schfer, S. (2019). Tools of the trade: practices and politics of researching the future in climate engineering. *Sustainability Science*, 14(4), 953–962. Retrieved from <https://doi.org/10.1007/s11625-019-00692-x> doi: 10.1007/s11625-019-00692-x
- MacMartin, D. G., Keith, D. W., Kravitz, B., & Caldeira, K. (2013). Management of trade-offs in geoengineering through optimal choice of non-uniform radiative forcing. *Nature Climate Change*, 3(4), 365–368. Retrieved from <https://doi.org/10.1038/nclimate1722> doi: 10.1038/nclimate1722
- MacMartin, D. G., & Kravitz, B. (2019). Mission-driven research for stratospheric aerosol geoengineering. *Proceedings of the National Academy of Sciences*, 116(4), 1089–1094. doi: 10.1073/pnas.1811022116
- MacMartin, D. G., Kravitz, B., Mills, M. J., Tribbia, J. J., Tilmes, S., Richter, J. H., ... Lamarque, J.-F. (2017). The Climate Response to Stratospheric Aerosol Geoengineering Can Be Tailored Using Multiple Injection Locations. *Journal of Geophysical Research: Atmospheres*, 122(23), 12,574–12,590. doi: 10.1002/2017jd026868
- MacMartin, D. G., Wang, W., Richter, J. H., Mills, M. J., Kravitz, B., & Tilmes, S. (2019). Timescale for Detecting the Climate Response to Stratospheric Aerosol Geoengineering. *Journal of Geophysical Research: Atmospheres*, 1233–1247. doi: 10.1029/2018jd028906
- Madronich, S., Tilmes, S., Kravitz, B., MacMartin, D. G., & Richter, J. H. (2018). Response of surface ultraviolet and visible radiation to stratospheric SO₂ injections. *Atmosphere*, 9(11). doi: 10.3390/atmos9110432
- Matte, D., Larsen, M. A. D., Christensen, O. B., & Christensen, J. H. (2019). Robustness and scalability of regional climate projections over europe. *Frontiers in Environmental Science*, 6, 163. Retrieved from <https://www.frontiersin.org/article/10.3389/fenvs.2018.00163> doi: 10.3389/fenvs.2018.00163
- McIlhattan, E. A., Lacoyer, T. S., & Miller, N. B. (2017, 05). Observational Evidence Linking Arctic Supercooled Liquid Cloud Biases in CESM to Snowfall Processes. *Journal of Climate*, 30(12), 4477–4495. Retrieved from <https://doi.org/10.1175/JCLI-D-16-0666.1> doi: 10.1175/JCLI-D-16-0666.1
- Mercado, L. M., Bellouin, N., Sitch, S., Boucher, O., Huntingford, C., Wild, M., & Cox, P. M. (2009). Impact of changes in diffuse radiation on the global land carbon sink. *Nature*, 458(7241), 1014–1017.
- Merlis, T. M., & Henry, M. (2018, 06). Simple Estimates of Polar Amplification in Moist Diffusive Energy Balance Models. *Journal of Climate*, 31(15), 5811–5824. Retrieved from <https://doi.org/10.1175/JCLI-D-17-0578.1> doi: 10.1175/JCLI-D-17-0578.1
- Mills, M. J., Richter, J. H., Tilmes, S., Kravitz, B., Macmartin, D. G., Glanville, A. A., ... Kinnison, D. E. (2017). Radiative and chemical response to interactive stratospheric sulfate aerosols in fully coupled CESM1(WACCM). *Journal of Geophysical Research: Atmospheres*, 122(23), 13,061–13,078. doi: 10.1002/2017JD027006
- Mills, M. J., Schmidt, A., Easter, R., Solomon, S., Kinnison, D. E., Ghan, S. J., ... Gettelman, A. (2016). Global volcanic aerosol properties derived from emissions, 19902014, using CESM1(WACCM). *Journal of Geophysical Research: Atmospheres*, 121(5), 2332–2348. Retrieved from <https://agupubs.onlinelibrary.wiley.com/doi/abs/10.1002/2015JD024290> doi: 10.1002/2015JD024290
- Morgenstern, O., Stone, K. A., Schofield, R., Akiyoshi, H., Yamashita, Y., Kinnison, D. E., ... Chipperfield, M. P. (2018). Ozone sensitivity to vary-

- 855 ing greenhouse gases and ozone-depleting substances in CCMI-1 simu-
 856 lations. *Atmospheric Chemistry and Physics*, 18(2), 1091–1114. Re-
 857 tried from <https://www.atmos-chem-phys.net/18/1091/2018/> doi:
 858 10.5194/acp-18-1091-2018
- 859 Muller, C. J., & O’Gorman, P. A. (2011). An energetic perspective on the regional
 860 response of precipitation to climate change. *Nature Climate Change*, 1(5),
 861 266–271. Retrieved from <https://doi.org/10.1038/nclimate1169> doi:
 862 10.1038/nclimate1169
- 863 Niemeier, U., Richter, J. H., & Tilmes, S. (2020). Differing responses of the QBO
 864 to SO₂ injections in two global models. *Atmospheric Chemistry and Physics
 865 Discussions*, 2020, 1–21. Retrieved from [https://www.atmos-chem-phys
 866 -discuss.net/acp-2020-206/](https://www.atmos-chem-phys

 866 -discuss.net/acp-2020-206/) doi: 10.5194/acp-2020-206
- 867 Niemeier, U., & Schmidt, H. (2017). Changing transport processes in the strato-
 868 sphere by radiative heating of sulfate aerosols. *Atmospheric Chemistry and
 869 Physics*, 17(24), 14871–14886. Retrieved from [https://www.atmos-chem-phys.net/17/14871/2017/](https://www.atmos-chem-phys

 870 .net/17/14871/2017/) doi: 10.5194/acp-17-14871-2017
- 871 Niemeier, U., Schmidt, H., Alterskjær, K., & Kristjánsson, J. E. (2013). Solar ir-
 872 radiance reduction via climate engineering: Impact of different techniques
 873 on the energy balance and the hydrological cycle. *Journal of Geophysical
 874 Research: Atmospheres*, 118(21), 11,905–11,917. Retrieved from [https://
 876 agupubs.onlinelibrary.wiley.com/doi/abs/10.1002/2013JD020445](https://

 875 agupubs.onlinelibrary.wiley.com/doi/abs/10.1002/2013JD020445) doi:
 10.1002/2013JD020445
- 877 Norris, J. R., Allen, R. J., Evan, A. T., Zelinka, M. D., O’Dell, C. W., & Klein,
 878 S. A. (2016). Evidence for climate change in the satellite cloud record. *Nature*,
 536(7614), 72–75. Retrieved from <https://doi.org/10.1038/nature18273>
 doi: 10.1038/nature18273
- 879 Oschlies, A., Held, H., Keller, D., Keller, K., Mengis, N., Quaas, M., ... Schmidt,
 880 H. (2017). Indicators and metrics for the assessment of climate engineering.
 881 *Earth’s Future*, 5(1), 49–58. Retrieved from [https://agupubs.onlinelibrary
 883 .wiley.com/doi/abs/10.1002/2016EF000449](https://agupubs.onlinelibrary

 882 .wiley.com/doi/abs/10.1002/2016EF000449) doi: 10.1002/2016EF000449
- 884 Pitari, G., Aquila, V., Kravitz, B., Robock, A., Watanabe, S., Cionni, I., ... Tilmes,
 885 S. (2014). Stratospheric ozone response to sulfate geoengineering: Results from
 886 the geoengineering model intercomparison project (geomip). *Journal of Geo-
 887 physical Research: Atmospheres*, 119(5), 2629–2653. Retrieved from [https://
 889 agupubs.onlinelibrary.wiley.com/doi/abs/10.1002/2013JD020566](https://

 888 agupubs.onlinelibrary.wiley.com/doi/abs/10.1002/2013JD020566) doi:
 10.1002/2013JD020566
- 890 Polvani, L. M., Banerjee, A., & Schmidt, A. (2019). Northern hemisphere conti-
 891 nental winter warming following the 1991 Mt. Pinatubo eruption: reconciling
 892 models and observations. *Atmospheric Chemistry and Physics*, 19(9), 6351–
 893 6366. Retrieved from <https://www.atmos-chem-phys.net/19/6351/2019/>
 894 doi: 10.5194/acp-19-6351-2019
- 895 Richter, J. H., Tilmes, S., Mills, M. J., Tribbia, J. J., Kravitz, B., Macmartin, D. G.,
 896 ... Lamarque, J. F. (2017). Stratospheric dynamical response and ozone
 897 feedbacks in the presence of SO₂ injections. *Journal of Geophysical Research:
 898 Atmospheres*, 122(23), 12,557–12,573. doi: 10.1002/2017JD026912
- 899 Robock, A. (2000). Volcanic eruptions and climate. *Reviews of Geophysics*, 38(2),
 900 191–219. Retrieved from [https://agupubs.onlinelibrary.wiley.com/doi/
 902 abs/10.1029/1998RG000054](https://agupubs.onlinelibrary.wiley.com/doi/

 901 abs/10.1029/1998RG000054) doi: 10.1029/1998RG000054
- 903 Robock, A., & Mao, J. (1995). The volcanic signal in surface temperature obser-
 904 vations. *Journal of Climate*, 8(5), 1086–1103. Retrieved from [https://doi
 906 .org/10.1175/1520-0442\(1995\)008<1086:TVSIST>2.0.CO;2](https://doi

 905 .org/10.1175/1520-0442(1995)008<1086:TVSIST>2.0.CO;2) doi: 10.1175/
 1520-0442(1995)008<1086:TVSIST>2.0.CO;2
- 907 Russotto, R. D., & Ackerman, T. P. (2018a). Changes in clouds and thermo-
 908 dynamics under solar geoengineering and implications for required solar
 909 reduction. *Atmospheric Chemistry and Physics*, 18(16), 11905–11925. Re-

- trieved from <https://www.atmos-chem-phys.net/18/11905/2018/> doi: 10.5194/acp-18-11905-2018
- Russotto, R. D., & Ackerman, T. P. (2018b). Energy transport, polar amplification, and ITCZ shifts in the GeoMIP G1 ensemble. *Atmospheric Chemistry and Physics*, 18(3), 2287–2305. Retrieved from <https://www.atmos-chem-phys.net/18/2287/2018/> doi: 10.5194/acp-18-2287-2018
- Schmidt, A., Mills, M. J., Ghan, S., Gregory, J. M., Allan, R. P., Andrews, T., ... Toon, O. B. (2018). Volcanic radiative forcing from 1979 to 2015. *Journal of Geophysical Research: Atmospheres*, 123(22), 12491–12508. Retrieved from <https://agupubs.onlinelibrary.wiley.com/doi/abs/10.1029/2018JD028776> doi: 10.1029/2018JD028776
- Simpson, I., Hitchcock, P., Seager, R., Wu, Y., & Callaghan, P. (2018). The downward influence of uncertainty in the northern hemisphere stratospheric polar vortex response to climate change. *Journal of Climate*, 31(16), 6371–6391. Retrieved from <https://doi.org/10.1175/JCLI-D-18-0041.1> doi: 10.1175/JCLI-D-18-0041.1
- Simpson, I., Tilmes, S., Richter, J., Kravitz, B., MacMartin, D., Mills, M., ... Pendergrass, A. (2019). The regional hydroclimate response to stratospheric sulfate geoengineering and the role of stratospheric heating. *Journal of Geophysical Research: Atmospheres*, 2019JD031093. Retrieved from <https://onlinelibrary.wiley.com/doi/abs/10.1029/2019JD031093> doi: 10.1029/2019JD031093
- Smyth, J. E., Russotto, R. D., & Storelvmo, T. (2017). Thermodynamic and dynamic responses of the hydrological cycle to solar dimming. *Atmospheric Chemistry and Physics*, 17(10), 6439–6453. Retrieved from <https://www.atmos-chem-phys.net/17/6439/2017/> doi: 10.5194/acp-17-6439-2017
- Song, X.-P., Hansen, M. C., Stehman, S. V., Potapov, P. V., Tyukavina, A., Vermote, E. F., & Townshend, J. R. (2018). Global land change from 1982 to 2016. *Nature*, 560(7720), 639–643. Retrieved from <https://doi.org/10.1038/s41586-018-0411-9> doi: 10.1038/s41586-018-0411-9
- Tavoni, M., Bosetti, V., Shayegh, S., Drouet, L., Emmerling, J., Fuss, S., ... Rickels, W. (2017). Challenges and opportunities for integrated modeling of climate engineering. *FEEM Working Paper*(38). doi: <http://dx.doi.org/10.2139/ssrn.3035166>
- Taylor, K. E. (2001). Summarizing multiple aspects of model performance in a single diagram. *Journal of Geophysical Research: Atmospheres*, 106(D7), 7183–7192. Retrieved from <https://agupubs.onlinelibrary.wiley.com/doi/abs/10.1029/2000JD900719> doi: 10.1029/2000JD900719
- Tilmes, S., MacMartin, D. G., Lenaerts, J. T. M., van Kampenhout, L., Muntjewerf, L., Xia, L., ... Robock, A. (2020). Reaching 1.5 and 2.0C global surface temperature targets using stratospheric aerosol geoengineering. *Earth System Dynamics*, 11(3), 579–601. Retrieved from <https://esd.copernicus.org/articles/11/579/2020/> doi: 10.5194/esd-11-579-2020
- Tilmes, S., Müller, R., & Salawitch, R. (2008). The sensitivity of polar ozone depletion to proposed geoengineering schemes. *Science*, 320(5880), 1201–1204. Retrieved from <https://science.sciencemag.org/content/320/5880/1201> doi: 10.1126/science.1153966
- Tilmes, S., Richter, J. H., Kravitz, B., MacMartin, D. G., Mills, M. J., Simpson, I. R., ... Ghosh, S. (2018). CESM1(WACCM) stratospheric aerosol geoengineering large ensemble project. *Bulletin of the American Meteorological Society*(11), 2361–2371. doi: 10.1175/BAMS-D-17-0267.1
- Tilmes, S., Richter, J. H., Mills, M. J., Kravitz, B., MacMartin, D. G., Garcia, R. R., ... Vitt, F. (2018). Effects of Different Stratospheric SO₂ Injection Altitudes on Stratospheric Chemistry and Dynamics. *Journal of Geophysical Research: Atmospheres*, 123(9), 4654–4673. doi: 10.1002/2017JD028146

- 965 Tilmes, S., Richter, J. H., Mills, M. J., Kravitz, B., Macmartin, D. G., Vitt, F.,
 966 ... Lamarque, J. F. (2017). Sensitivity of aerosol distribution and climate
 967 response to stratospheric SO₂ injection locations. *Journal of Geophysical
 968 Research: Atmospheres*, 122(23), 12,591–12,615. doi: 10.1002/2017JD026888
- 969 Timmreck, C., Mann, G. W., Aquila, V., Hommel, R., Lee, L. A., Schmidt, A.,
 970 ... Weisenstein, D. (2018). The interactive stratospheric aerosol model
 971 intercomparison project (ISA-MIP): motivation and experimental de-
 972 sign. *Geoscientific Model Development*, 11(7), 2581–2608. Retrieved
 973 from <https://gmd.copernicus.org/articles/11/2581/2018/> doi:
 974 10.5194/gmd-11-2581-2018
- 975 van Kampenhout, L., Lenaerts, J. T. M., Lipscomb, W. H., Lhermitte, S., Nol, B.,
 976 Vizcano, M., ... van den Broeke, M. R. (2020). Present-day greenland ice
 977 sheet climate and surface mass balance in CESM2. *Journal of Geophysical Re-
 978 search: Earth Surface*, 125(2), e2019JF005318. Retrieved from <https://agupubs.onlinelibrary.wiley.com/doi/abs/10.1029/2019JF005318>
 979 (e2019JF005318 10.1029/2019JF005318) doi: 10.1029/2019JF005318
- 980 Vattioni, S., Weisenstein, D., Keith, D., Feinberg, A., Peter, T., & Stenke, A.
 981 (2019). Exploring accumulation-mode H₂SO₄ versus SO₂ stratospheric sul-
 982 fate geoengineering in a sectional aerosol-chemistry-climate model. *Atmo-
 983 spheric Chemistry and Physics*, 19(7), 4877–4897. Retrieved from <https://www.atmos-chem-phys.net/19/4877/2019/> doi: 10.5194/acp-19-4877-2019
- 984 Visioni, D., MacMartin, D. G., Kravitz, B., Lee, W., Simpson, I. R., & Richter,
 985 J. H. (2020). Reduced poleward transport due to stratospheric heating under
 986 stratospheric aerosols geoengineering. *Geophysical Research Letters*, n/a(n/a),
 987 e2020GL089470. Retrieved from <https://agupubs.onlinelibrary.wiley.com/doi/abs/10.1029/2020GL089470> (e2020GL089470 2020GL089470) doi:
 988 10.1029/2020GL089470
- 989 Visioni, D., MacMartin, D. G., Kravitz, B., Richter, J. H., Tilmes, S., & Mills, M. J.
 990 (2020). Seasonally modulated stratospheric aerosol geoengineering alters the
 991 climate outcomes. *Geophysical Research Letters*, n/a(n/a), e2020GL088337.
 992 Retrieved from <https://agupubs.onlinelibrary.wiley.com/doi/abs/10.1029/2020GL088337> (e2020GL088337 2020GL088337) doi: 10.1029/
 993 2020GL088337
- 994 Visioni, D., MacMartin, D. G., Kravitz, B., Tilmes, S., Mills, M. J., Richter, J. H.,
 995 & Boudreau, M. P. (2019). Seasonal injection strategies for stratospheric
 996 aerosol geoengineering. *Geophysical Research Letters*, 46(13), 7790–7799.
 997 Retrieved from <https://agupubs.onlinelibrary.wiley.com/doi/abs/10.1029/2019GL083680> doi: 10.1029/2019GL083680
- 1000 Visioni, D., Pitari, G., & Aquila, V. (2017). Sulfate geoengineering: A review of the
 1001 factors controlling the needed injection of sulfur dioxide. *Atmospheric Chem-
 1002 istry and Physics*. doi: 10.5194/acp-17-3879-2017
- 1003 Visioni, D., Pitari, G., Aquila, V., Tilmes, S., Cionni, I., Di Genova, G., & Mancini,
 1004 E. (2017). Sulfate geoengineering impact on methane transport and life-
 1005 time: results from the geoengineering model intercomparison project (Ge-
 1006 oMIP). *Atmospheric Chemistry and Physics*, 17(18), 11209–11226. Re-
 1007 tried from <https://www.atmos-chem-phys.net/17/11209/2017/> doi:
 1008 10.5194/acp-17-11209-2017
- 1009 Visioni, D., Pitari, G., Di Genova, G., Tilmes, S., & Cionni, I. (2018). Upper tro-
 1010 pospheric ice sensitivity to sulfate geoengineering. *Atmospheric Chemistry and
 1011 Physics*. doi: 10.5194/acp-18-14867-2018
- 1012 Visioni, D., Pitari, G., Tuccella, P., & Curci, G. (2018). Sulfur deposition changes
 1013 under sulfate geoengineering conditions: Quasi-biennial oscillation effects on
 1014 the transport and lifetime of stratospheric aerosols. *Atmospheric Chemistry and
 1015 Physics*. doi: 10.5194/acp-18-2787-2018
- 1016 Visioni, D., Slessarev, E., MacMartin, D., Mahowald, N. M., Goodale, C. L., & Xia,
 1017

Accepted Article

- 1020 L. (2020). What goes up must come down: impacts of deposition in a sulfate
1021 geoengineering scenario. *Environmental Research Letters*, 15(9). Retrieved
1022 from <http://iopscience.iop.org/10.1088/1748-9326/ab94eb>
- 1023 Xia, L., Nowack, P. J., Tilmes, S., & Robock, A. (2017). Impacts of stratospheric
1024 sulfate geoengineering on tropospheric ozone. *Atmospheric Chemistry and*
1025 *Physics*, 17(19), 11913–11928. Retrieved from [https://www.atmos-chem-phys](https://www.atmos-chem-phys.net/17/11913/2017/)
1026 .net/17/11913/2017/ doi: 10.5194/acp-17-11913-2017

1 TEMPERATURE TARGET

(3) 1x1 SD

Role of different temperature targets

What are we missing if we “turn down the sun” as a proxy for a more complex SS strategy?

(3) 1x1 SS

(3) 3x3 SD

What if we turn down the sun in a more congruent way?

(20) 3x3 SS

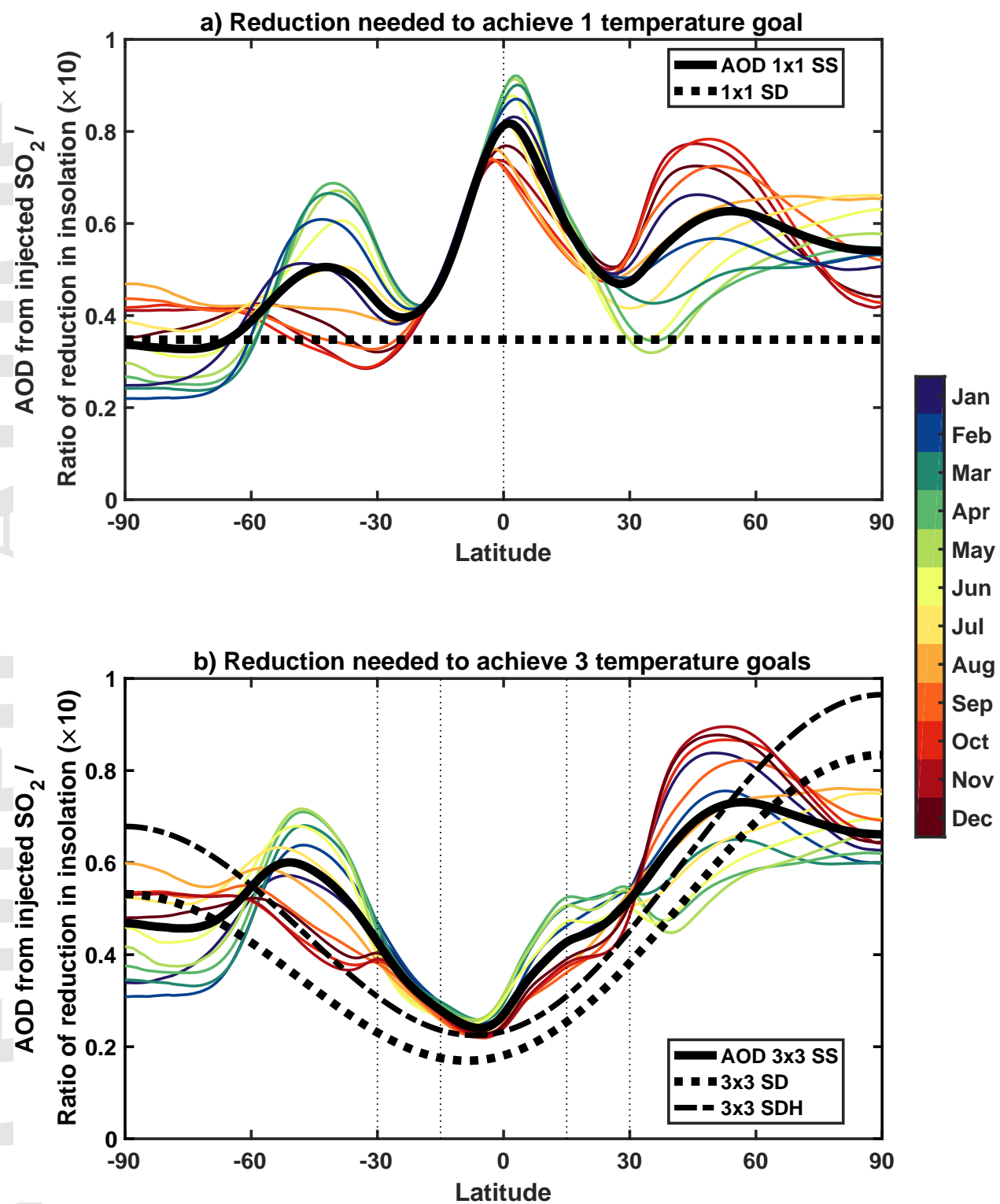
Role of stratospheric heating

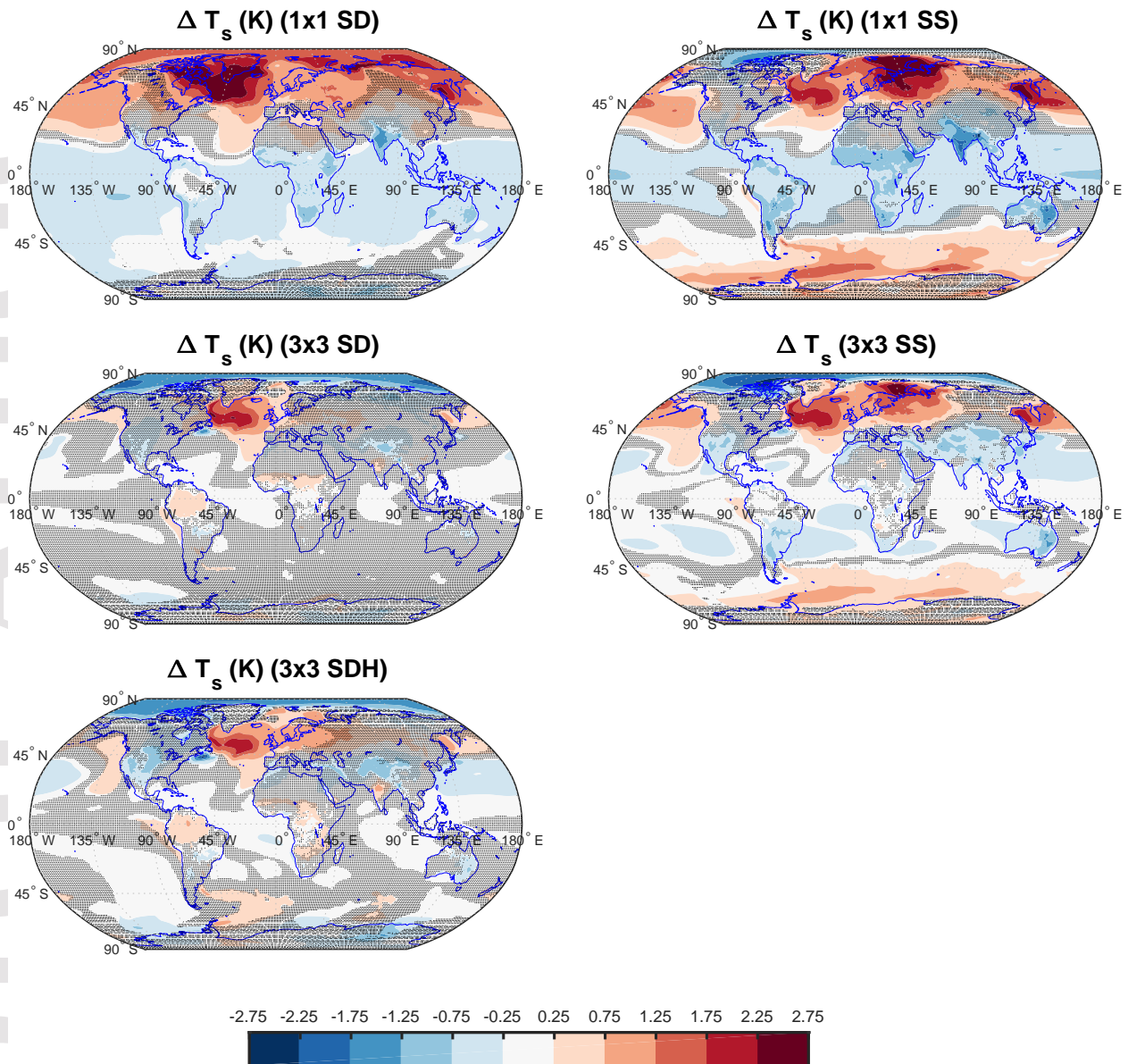
Role of seasonal variations in the reduced sunlight

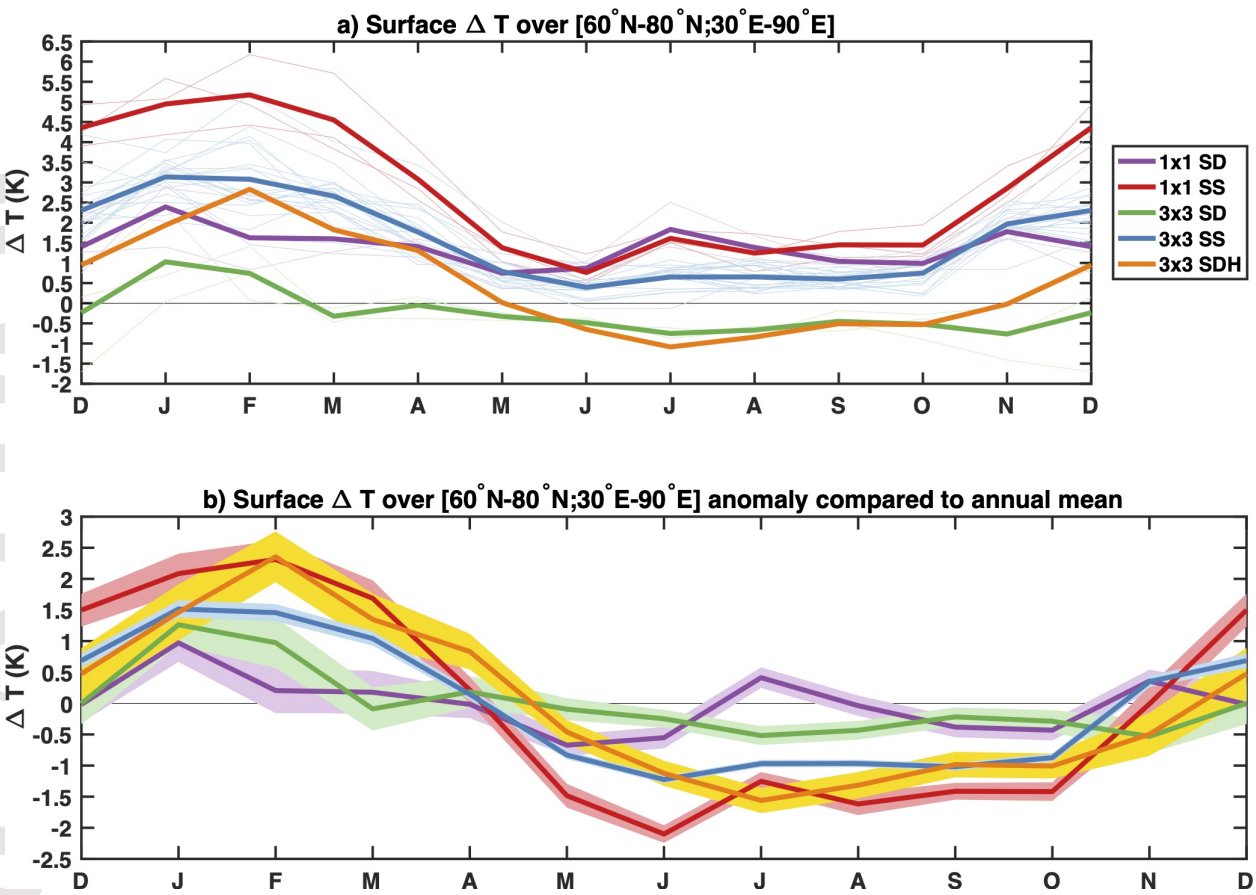
(3) 3x3 SDH

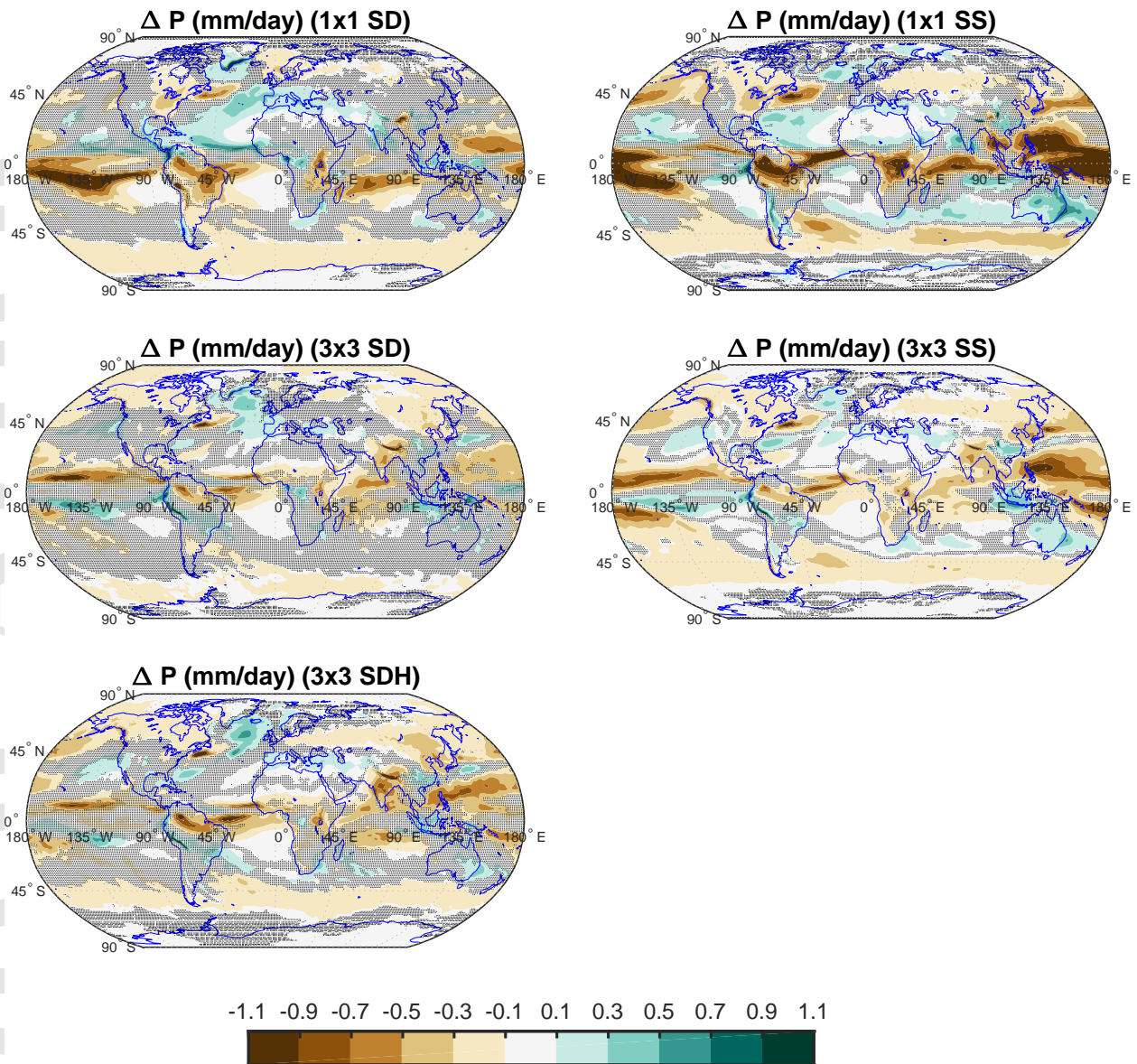
Role of diffuse radiation

3 TEMPERATURE TARGET

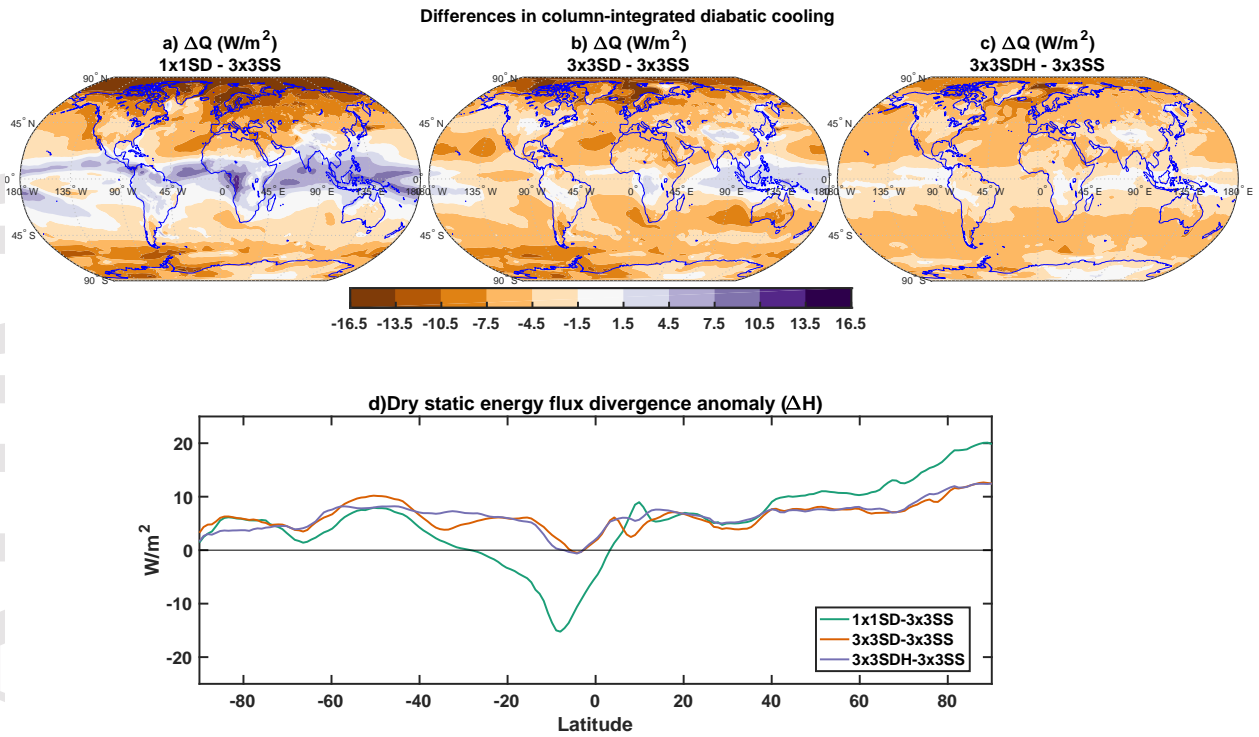


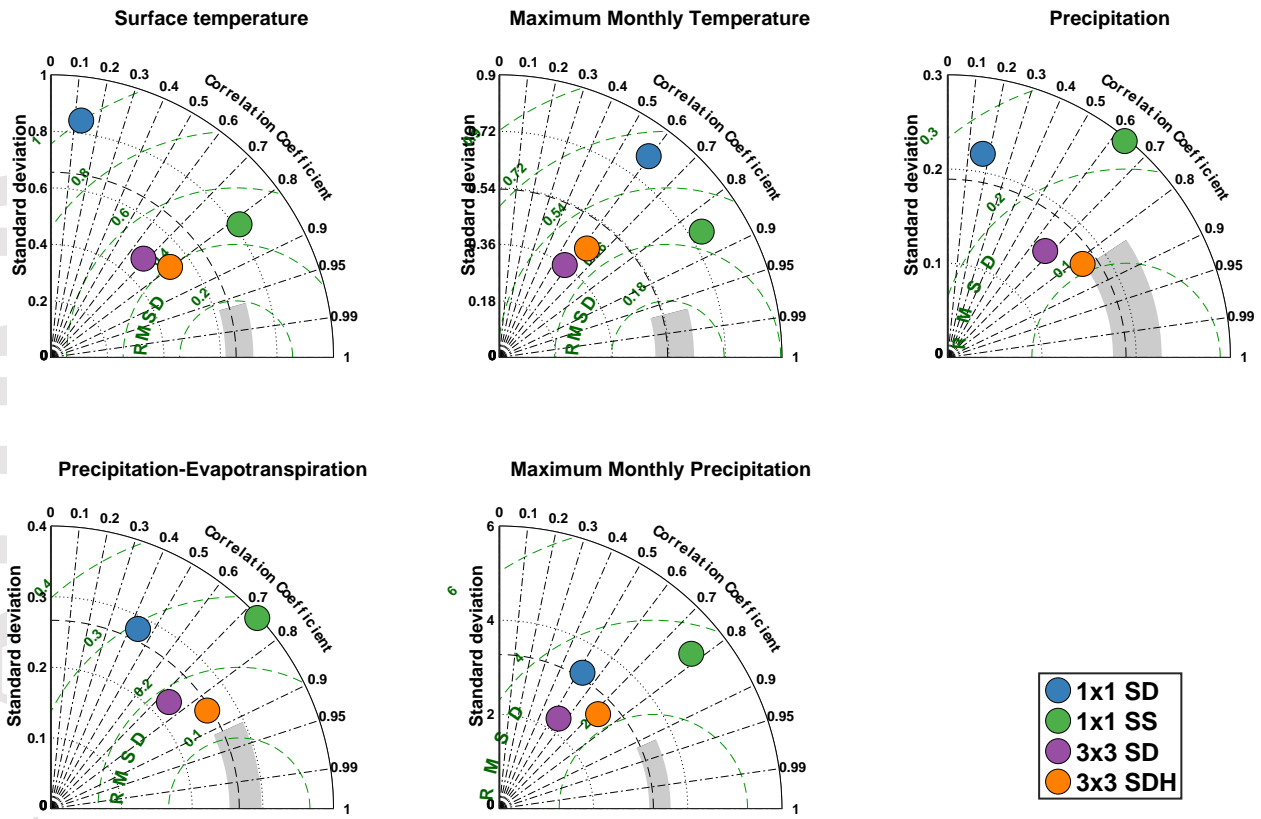




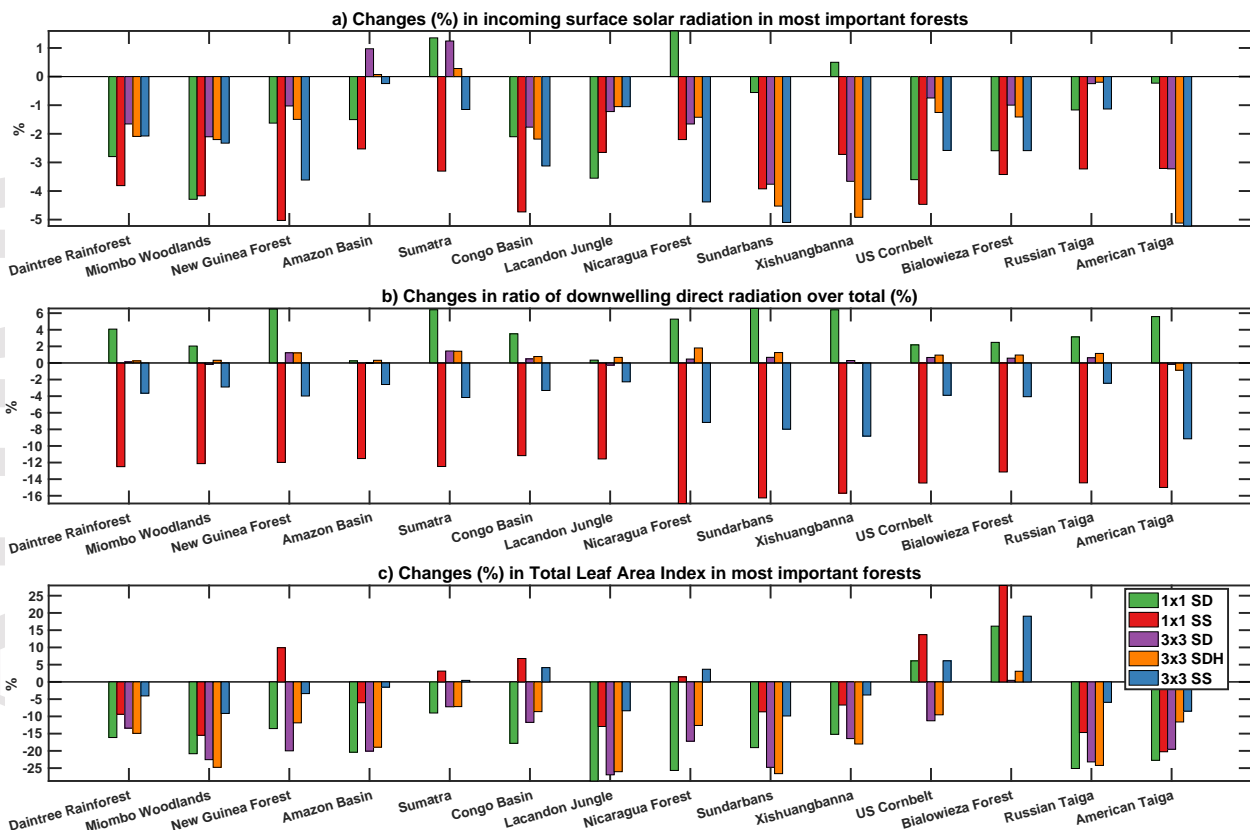


Accepted

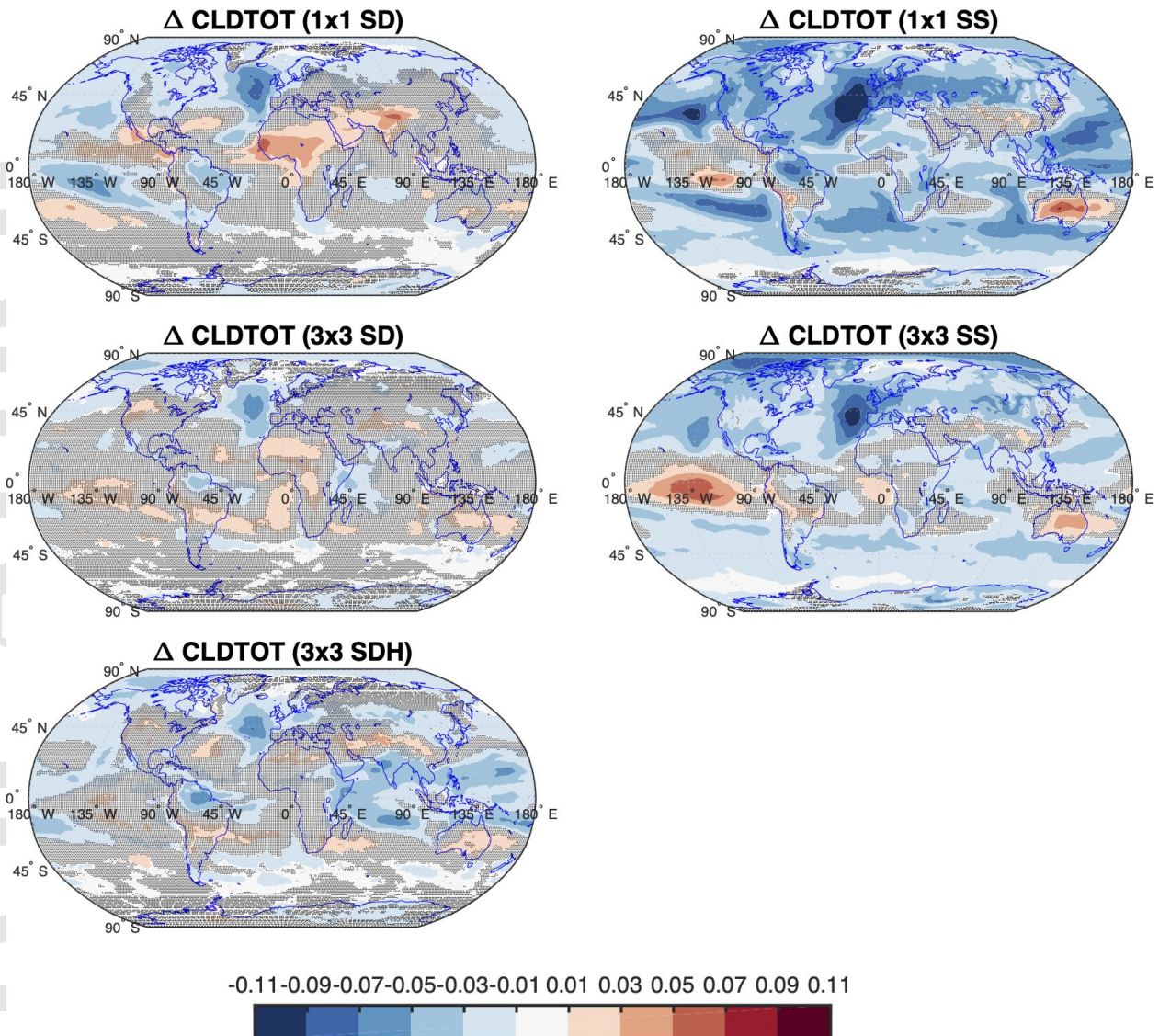




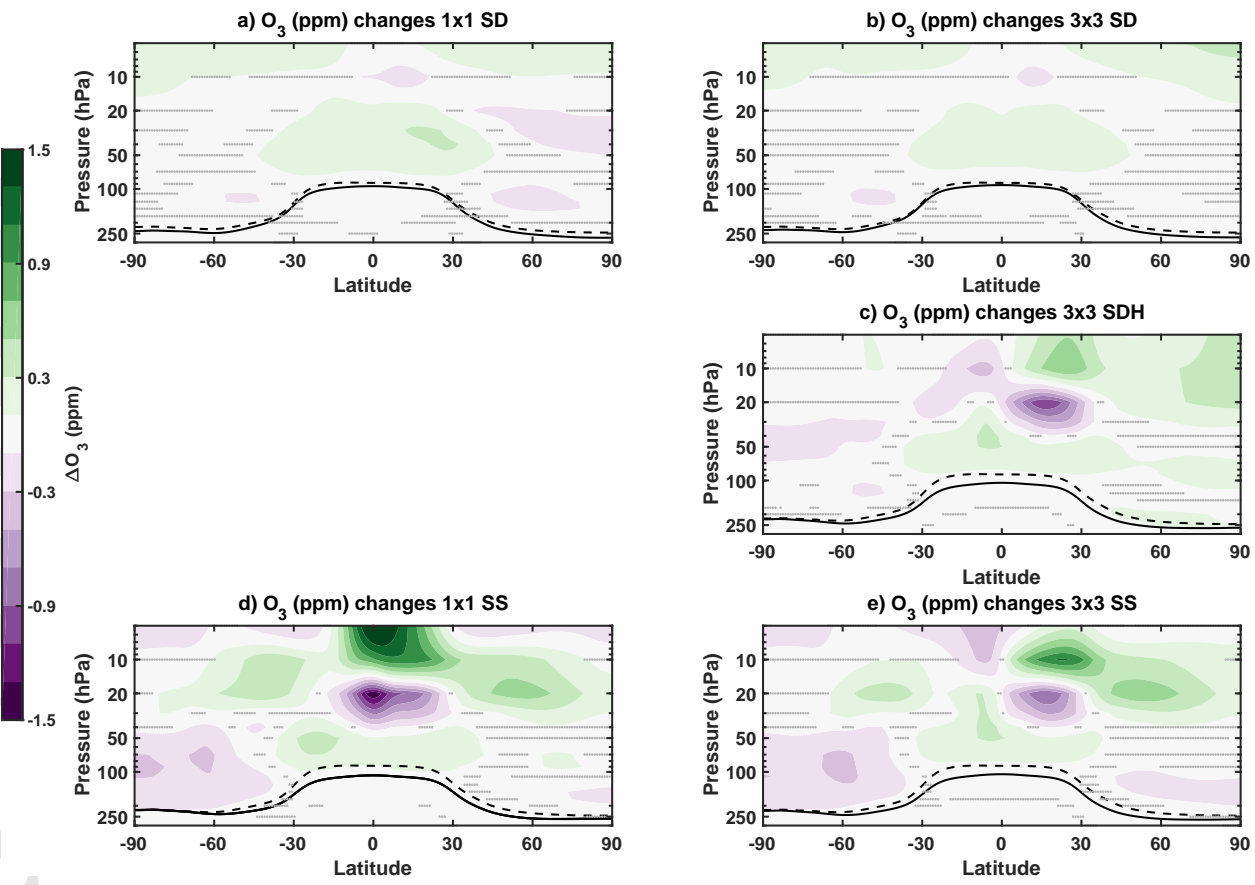
Accepted Article



Accepted Article



Accepted Article



What are we missing by using solar dimming as a proxy for sulfate geoengineering?

